

Robust nonlinear control of close formation flight

Qingrui Zhang¹ and Hugh H. T. Liu²

University of Toronto, Toronto, Ontario M3H 5T6, Canada

This paper investigates the robust nonlinear close formation control problem. It aims to achieve precise position control at dynamic flight operation for a follower aircraft under the aerodynamic impact due to the trailing vortices generated by a leader aircraft. One crucial concern is the control robustness that ensures the boundedness of position error subject to uncertainties and disturbances to be regulated with accuracy. This paper develops a robust nonlinear formation control algorithm to fulfill precise close formation tracking control. The proposed control algorithm consists of baseline control laws and disturbance observers. The baseline control laws are employed to stabilize the nonlinear dynamics of close formation flight, while the disturbance observers are introduced to compensate system uncertainties and formation-related aerodynamic disturbances. The position control performance can be guaranteed within the desired boundedness to harvest enough drag reduction for a follower aircraft in close formation using the proposed design. The efficacy of the proposed design is demonstrated via numerical simulations of close formation flight of two aircraft.

¹ qingrui.zhang@mail.utoronto.ca

² liu@utias.utoronto.ca

Nomenclature

b	= Wing span
C_{IW}	= Rotation matrix from a wind frame to the inertial frame
c_i	= Control parameter ($i = V, \chi, p, q, r$)
d_i	= System uncertainties and disturbances ($i = V, \gamma, \chi, \mu, \alpha, \beta, p, q, r$)
\widehat{d}_i	= Estimate of system uncertainties and disturbances
I_x, I_{xz}, I_y, I_z	= Moments of inertia
K_i	= Control parameter ($i = x, z, V, \gamma, \chi, \mu, \alpha, \beta, p, q, r$)
L, D, Y, T	= Lift, drag, side force, and thrust, respectively
$\mathcal{L}, \mathcal{M}, \mathcal{N}$	= Rolling, pitching, and yawing moments
l_x, l_y, l_z	= The optimal relative positions in the inertial frame
m_f	= Mass of the follower aircraft
p, q, r	= Angular rates in the body frame
r_x, r_y	= The optimal relative positions in the wind frame of the leader aircraft
T_i	= Time constant ($i = V, \gamma, \chi, W_x, W_y, W_z, \mu, \alpha, \beta, p, q, r$)
V_i, γ_i, χ_i	= Airspeed, flight path angle, and heading angle, respectively ($i = c, d, f, l, r$)
$\widehat{V}_f, \widehat{\gamma}_f, \widehat{\chi}_f$	= Resultant airspeed, flight path angle, and heading angle in trailing vortices
W_x, W_y, W_z	= Wake velocities induced by trailing vortices
$\widehat{W}_x, \widehat{W}_y, \widehat{W}_z$	= Estimates of wake velocities
x_i, y_i, z_i	= Position coordinates ($i = d, f, l, c$)
x_e, y_e, z_e	= Position errors in the inertial frame
α, β, μ	= Angle of attack, sideslip angle, and bank angle, respectively
$\Delta L, \Delta D, \Delta Y$	= Vortex-induced lift, drag, and side force, respectively
$\Delta \mathcal{L}, \Delta \mathcal{M}, \Delta \mathcal{N}$	= Vortex-induced moments
$\delta_a, \delta_e, \delta_r$	= Aileron, elevator, and rudder
ζ_i	= Damping ratio ($i = l_x, l_y, l_z, V, \gamma, \mu, \alpha, \beta$)
λ_i	= States of disturbance observer ($i = V, \gamma, \chi, W_x, W_y, W_z, \mu, \alpha, \beta, p, q, r$)
ξ_i	= Auxiliary signals ($i = x, z, \mu, \alpha, \beta$)
ω_i	= Natural frequencies ($i = l_x, l_y, l_z, V, \gamma, \mu, \alpha, \beta$)

Subscripts:

c = Command signal

d = Desired signal

I. Introduction

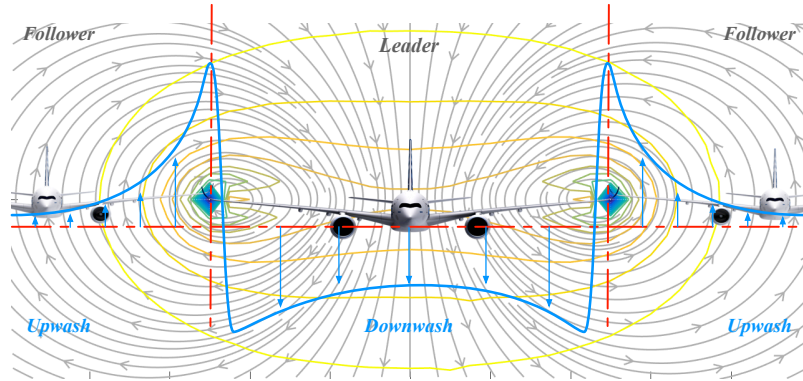


Fig. 1 Close formation flight

Close formation flight is inspired by migratory birds who adopt a “V-shape” formation flight when migrating from one habitat to another [1–3]. In close formation, a follower aircraft, holding a close relative position to a leader aircraft, flies in the upwash wake region of the trailing vortices induced by the leader aircraft as shown in Figure 1, by which the follower aircraft reduces its drag and thus saves fuels. Drag reduction of close formation flight has been demonstrated by simulations [4–6], observed by wind tunnel experiments [7, 8], and confirmed by flight tests [9–12].

Despite its benefits, close formation flight is challenging in terms of the accuracy and robustness requirement for guidance and control [6]. The position control accuracy must be guaranteed within the consideration of system uncertainties and formation-related aerodynamic disturbances. Yet, different control algorithms have been proposed for close formation flight. Most of them are focused on level and straight flight with constant speeds [13–16]. Two different linear strategies were applied, namely formation holding control and formation tracking control. Both of them are limited. Formation-holding control assumes a follower aircraft is initially well-trimmed at its optimal position in close formation, such as the proportional-integral (PI) formation control [14], the close formation control by the linear-quadratic regulator (LQR) [15], and the linear model predictive control (MPC)-based control [16]. Linear formation-tracking control doesn’t require the follower aircraft to

be initially located at its desired position in close formation [17–22], but they are not guaranteed to address complex nonlinear aircraft dynamics at dynamic flight operation. Additionally, linear control methods will experience dramatic performance degradation or even fail to stabilize the system, when being applied to nonlinear systems. Robust nonlinear formation control is, therefore, more preferable to accommodate close formation flight at dynamic operation.

Nonlinear close formation control is challenging. Contrary to linear cases, model uncertainties and aerodynamic disturbances are less predictable and harder to be described at nonlinear scenarios, making close formation control more difficult. Early robust nonlinear close formation control was investigated using sliding model control [23] or high order sliding mode (HOSM) control [24]. Both of the two methods only focus on outer-loop design, and they require the vortex-upper bounds of induced forces or their derivatives to satisfy certain limits to guarantee the stability. The nonlinear robust formation design including both inner-loop and outer-loop control was reported in [25] using an incremental nonlinear dynamic inversion (INDI) method, but this method is not robust to model uncertainties and external disturbances. Therefore, present nonlinear methods either rely on unknown model information to ensure both stability and robustness like the sliding mode control [24], or not robust to model uncertainties and external disturbances at general dynamic operations, such as the INDI-based control [25]. Therefore, it is still an open issue for nonlinear robust close formation control with certain performance guaranty only using available model information.

In this paper, we investigate the robust nonlinear control problem for close formation flight at dynamic operation. The control design is presented under a leader-following architecture. The fundamental objective is to secure highly precise position control for close formation flight at dynamic flight operation design with the consideration of system uncertainties and aerodynamic impact caused by trailing vortices of leader aircraft a robust nonlinear controller. Control robustness will be one of the critical concerns which significantly affects the possible accuracy for close formation flight as it is subject to system uncertainties and aerodynamic disturbances. A robust nonlinear formation controller, which consists of baseline controllers and disturbance observers, is proposed in this paper. The baseline controllers are designed based on a command filtered backstepping technique to stabilize the nominal nonlinear dynamics of an aircraft in close formation [26, 27],

whereas the disturbance observers could estimate and compensate for system uncertainties and formation-related aerodynamic disturbances by purely observing system inputs and available states. In the proposed design, the follower aircraft is required to track its dynamic optimal relative position to a leader aircraft in the inertial frame under different flight maneuvers. Both the inner-loop and outer-loop control will be studied in this paper, which makes the formation control design more reliably but also more difficult. The assumption on a well-designed inner-loop controller in [28] is, therefore, removed in this paper. The proposed design is capable of achieving highly accurate and efficiently robust control performance without using any gradient or boundary information of formation aerodynamic disturbances. Position tracking errors will be ultimately bounded. The final boundaries could be regulated by choosing different control parameters.

The rest of the paper is organized as follows. Section II presents some preliminaries, while Section III formulates reference trajectories. In Section IV, robust nonlinear control is reported and analyzed. Numerical simulations are given in Section V. Conclusions are in Section VI.

II. Preliminaries

Some preliminaries are provided, which will be used for the design and analysis in the sequel.

Definition 1 (Definition 4.6 [29]). *A system $\dot{\mathbf{x}} = \mathbf{f}(t, \mathbf{x})$ is uniformly ultimately bounded if there are positive constants \mathcal{A}_b and \mathcal{A}_c , there exists $\mathcal{T} = \mathcal{T}(\mathcal{A}_a, \mathcal{A}_b)$ for any $\mathcal{A}_a \in (0, \mathcal{A}_c)$, such that*

$$\|\mathbf{x}(t_0)\| \leq \mathcal{A}_a \Rightarrow \|\mathbf{x}(t)\| \leq \mathcal{A}_b, \quad \forall t \geq t_0 + \mathcal{T} \quad (1)$$

Lemma 1. *Let $d(t)$ be a bounded signal whose derivative $\dot{d}(t)$, namely $d(t) \in \mathcal{L}_\infty$ and $\dot{d}(t) \in \mathcal{L}_\infty$. Assume $\hat{d}(t)$ is the estimation of $d(t)$ through a first-order filter as shown in (2).*

$$\mathcal{T}_d \dot{\hat{d}} = -\hat{d} + d \quad (2)$$

where $\mathcal{T}_d > 0$ is a time constant. Define $\tilde{d} = \hat{d} - d$ as the estimation error. If $\hat{d}(0) = 0$,

1. \tilde{d} are globally bounded by $|\tilde{d}| \leq \max\{|d(0)|, \mathcal{T}_d \|\dot{d}\|_\infty\}$;
2. if $|d(0)| \neq \mathcal{T}_d \|\dot{d}\|_\infty$, there exist any small positive constant ϵ and time t_ϵ such that $|\tilde{d}| < \mathcal{T}_d \|\dot{d}\|_\infty + \epsilon$ for all $t > t_\epsilon$, where $t_\epsilon = \max\left\{0, \mathcal{T}_d \ln\left(\frac{|d(0)| - \mathcal{T}_d \|\dot{d}\|_\infty}{\epsilon}\right)\right\}$;
3. if $\lim_{t \rightarrow \infty} \dot{d} = 0$, $\lim_{t \rightarrow \infty} \tilde{d} = 0$.

III. Formulation of reference trajectories at dynamic operation

In this section, a motion planner is designed for follower aircraft at close formation. According to [6], the optimal relative position in close formation is static in the wind frame of the leader aircraft. Assume $[r_x, r_y, 0]^T$ is the static optimal relative position in the wind frame of the leader aircraft, where r_x ranges from $-2b$ to $-10b$ and r_y is around $\pm 0.95b$ with b denoting the wing span. When flying at close formation, the reference position of a follower aircraft in the inertial frame is

$$x_d = x_l + l_x, \quad y_d = y_l + l_y, \quad \text{and} \quad z_d = z_l + l_z \quad (3)$$

where x_l , y_l , and z_l are position coordinates of the leader aircraft in the inertial frame, and $[l_x, l_y, l_z]^T = \mathbf{C}_{IW}(\mu_l, \gamma_l, \chi_l)[r_x, r_y, 0]^T$ where μ_l , γ_l , and χ_l are the bank, flight path, and heading angles of the leader aircraft. Differentiating (3) yields

$$\dot{x}_d = V_l \cos \gamma_l \cos \chi_l + \dot{l}_x, \quad \dot{y}_d = V_l \cos \gamma_l \sin \chi_l + \dot{l}_y, \quad \text{and} \quad \dot{z}_d = -V_l \sin \gamma_l + \dot{l}_z \quad (4)$$

where V_l , γ_l , and χ_l are the airspeed, flight path angle, and heading angle of leader aircraft, respectively. At dynamic operation, l_x , l_y , and l_z are time-varying, but their derivatives cannot be accurately computed. Hence, in the design, we introduce a command filter (5) to get the command signals l_{ci} and \dot{l}_{ci} ($i \in \{x, y, z\}$). Let $\mathcal{S}(t)$ be a smooth signal, so the command filter is

$$\begin{bmatrix} \dot{\mathcal{J}}_c \\ \ddot{\mathcal{J}}_c \end{bmatrix} = \underbrace{\begin{bmatrix} 0 & 1 \\ -\omega_{\mathcal{J}}^2 & -2\zeta_{\mathcal{J}}\omega_{\mathcal{J}} \end{bmatrix}}_{\mathbf{A}_{\mathcal{J}}} \begin{bmatrix} \mathcal{J}_c \\ \dot{\mathcal{J}}_c \end{bmatrix} + \begin{bmatrix} 0 \\ \omega_{\mathcal{J}}^2 \end{bmatrix} \mathcal{S}(t) \quad (5)$$

where $\omega_{\mathcal{J}} > 0$ is the natural frequency and $\zeta_{\mathcal{J}} > 0$ is the damping ratio. Let $\tilde{\mathcal{J}} = \mathcal{J}_c - \mathcal{S}$ and $\mathbf{e}_{\mathcal{J}} = [\tilde{\mathcal{J}}, \dot{\tilde{\mathcal{J}}}]^T$. If $\mathcal{J}_c(0) = \mathcal{S}(0)$ and $\dot{\mathcal{J}}_c(0) = 0$, Lemma 2 exists for any bounded signal $\mathcal{S}(t)$.

Lemma 2. *The estimator (5) is input-to-state stable with respect to $\mathcal{S}(t)$. If both $\dot{\mathcal{J}}(t)$ and $\ddot{\mathcal{J}}(t)$ are bounded, $\tilde{\mathcal{J}}$ is uniformly and ultimately bounded, and the following inequality exists for $\mathbf{e}_{\mathcal{J}}(t)$.*

$$\|\mathbf{e}_{\mathcal{J}}\|_2 \leq \sqrt{\frac{\lambda_{\max}(\mathbf{P}_{\mathcal{J}})}{\lambda_{\min}(\mathbf{P}_{\mathcal{J}})}} e^{-\frac{t}{2\lambda_{\max}(\mathbf{P}_{\mathcal{J}})}} |\dot{\mathcal{J}}(0)| + \left(1 - e^{-\frac{t}{2\lambda_{\max}(\mathbf{P}_{\mathcal{J}})}}\right) \frac{2\lambda_{\max}^2(\mathbf{P}_{\mathcal{J}}) \|\ddot{\mathcal{J}} + 2\zeta_{\mathcal{J}}\omega_{\mathcal{J}}\dot{\mathcal{J}}\|_{\infty}}{\lambda_{\min}(\mathbf{P}_{\mathcal{J}})}$$

where $\lambda_{\max}(\cdot)$ and $\lambda_{\min}(\cdot)$ are the maximum and minimum eigenvalues of a matrix, respectively,

$\mathbf{P}_{\mathcal{J}}$ is positive definite such that $\mathbf{P}_{\mathcal{J}}\mathbf{A}_{\mathcal{J}} + \mathbf{A}_{\mathcal{J}}^T\mathbf{P}_{\mathcal{J}} = -\mathbf{I}$. Furthermore, there exist

$$\tilde{\mathcal{J}} = \mathcal{O}(1/\omega_{\mathcal{J}}) \quad \text{and} \quad \dot{\tilde{\mathcal{J}}}/\omega_{\mathcal{J}} = \mathcal{O}(1/\omega_{\mathcal{J}})$$

where $\mathcal{O}(\cdot)$ is an order of magnitude notation [29].

In real flight, $\dot{\gamma}_l$, $\dot{\chi}_l$, and $\dot{\mu}_l$ and their derivatives are all bounded, so (5) is a valid choice to obtain l_{ci} and \dot{l}_{ci} ($i \in \{x, y, z\}$). In addition, Lemma 2 indicates that the command signals l_{ci} and \dot{l}_{ci} ($i \in \{x, y, z\}$) could be ensured to be arbitrarily close to their corresponding desired values l_i and \dot{l}_i by choosing proper command filter parameters. Note that $\mathcal{S}_c(0) = \mathcal{S}(0)$ is needed to avoid the peaking phenomenon (Page 613, [29]). If $\mathcal{S}_c(0) \neq \mathcal{S}(0)$, \mathcal{S}_c , the signal $\dot{\mathcal{S}}_c$ will transiently peak to $\mathcal{O}(\omega_{\mathcal{S}})$ before it exponentially decays, resulting in the so-called peaking phenomenon due to $\mathcal{S}_c(0) \neq \mathcal{S}(0)$. Without loss of generality, the following assumption is introduced.

Assumption 1. *The attitude signals γ_l , χ_l , and μ_l and their derivatives are all bounded.*

In light of (5), the command position for a follower aircraft in close formation is $x_r = x_l + l_{cx}$, $y_r = y_l + l_{cy}$, and $z_r = z_l + l_{cz}$, and accordingly,

$$\begin{cases} \dot{x}_r = \dot{x}_l + \dot{l}_{cx}, & \dot{y}_r = \dot{y}_l + \dot{l}_{cy} \sin \chi_r, & \dot{z}_r = \dot{z}_l + \dot{l}_{cz} \\ V_r = \sqrt{\dot{x}_r^2 + \dot{y}_r^2 + \dot{z}_r^2}, & \gamma_r = -\sin^{-1}\left(\frac{\dot{z}_r}{V_r}\right), & \chi_r = \chi_l + \sin^{-1}\left(\frac{-\dot{l}_{cx} \sin \chi_l + \dot{l}_{cy} \cos \chi_l}{V_r \cos \gamma_r}\right) \end{cases} \quad (6)$$

IV. Robust nonlinear formation control design

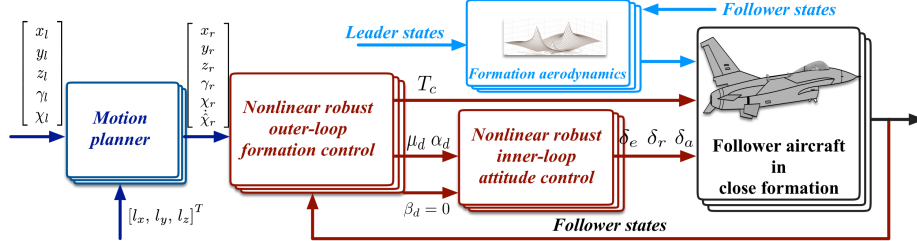


Fig. 2 The entire formation control structure

The proposed design in this section can be easily extended to the case with more than three aircraft, even though it is discussed under the leader-follower architecture with two aircraft. In the proposed design, command filtered backstepping technique is employed, which avoids the analytic calculation of time derivatives of intermediate virtual inputs [26, 27, 30, 31]. As shown in Figure 2, the entire design consists of two major loops: an outer loop for formation position control and an inner loop for attitude control. The outer-loop control allows a follower aircraft to track the planned motion by (6), and generates command thrust T_c , desired bank angle μ_d , and desired angle of attack α_d . The inner-loop control stabilizes follower aircraft's attitudes to their desired values μ_d and α_d from the outer-loop control, while holding zero sideslip angle β_f .

A. Outer-loop formation position control

Let \bar{D} and \bar{L} be the nominal values of the drag D and lift L , respectively. They are obtained by either available aerodynamic data or certain analytical models [32]. The sideslip angle β_f is negligibly small, as it is always stabilized to be zero. Accordingly, the side force Y is small and taken as a model uncertainty. The outer-loop dynamics used for control design are

$$\begin{cases} \dot{x}_f = V_f \cos \gamma_f \cos \chi_f + W_x \\ \dot{y}_f = V_f \cos \gamma_f \sin \chi_f + W_y \\ \dot{z}_f = -V_f \sin \gamma_f + W_z \end{cases} \quad \begin{cases} \dot{V}_f = \frac{1}{m_f} (T \cos \alpha_f \cos \beta_f - \bar{D}) - g \sin \gamma_f + d_V \\ \dot{\gamma}_f = \frac{(\bar{L} + T \sin \alpha_f) \cos \mu_f}{m_f V_f} - \frac{g}{V_f} \cos \gamma_f + d_\gamma \\ \dot{\chi}_f = \frac{(\bar{L} + T \sin \alpha_f) \sin \mu_f}{m_f V_f \cos \gamma_f} + d_\chi \end{cases} \quad (7)$$

where x_f , y_f , and z_f are follower position coordinates in the inertial frame, V_f is the airspeed, γ_f and χ_f are the flight path and heading angles, T is the thrust, W_x , W_y , and W_z are induced wake velocities, and d_V , d_γ , and d_χ are the augmentation of system uncertainties and disturbances.

$$\begin{cases} d_V = -\frac{D - \bar{D} + \Delta D}{m_f} - \frac{\dot{W}_{W_x}}{m_f} \\ d_\gamma = \frac{(L - \bar{L} + \Delta L) \cos \mu_f - (Y + \Delta Y - T \cos \alpha_f \sin \beta_f) \sin \mu_f}{m_f V_f} - \frac{\dot{W}_{W_y} \sin \mu_f + \dot{W}_{W_z} \cos \mu_f}{m_f V_f} \\ d_\chi = \frac{(L - \bar{L} + \Delta L) \sin \mu_f + (Y + \Delta Y - T \cos \alpha_f \sin \beta_f) \cos \mu_f}{m_f V_f \cos \gamma_f} + \frac{\dot{W}_{W_y} \cos \mu_f - \dot{W}_{W_z} \sin \mu_f}{m_f V_f \cos \gamma_f} \end{cases} \quad (8)$$

where \dot{W}_{W_x} , \dot{W}_{W_y} , and \dot{W}_{W_z} are the wake velocity derivatives denoted in the wind frame of follower aircraft, ΔL , ΔD , and ΔY are the vortex-induced forces. According to [6], W_x , W_y , and W_z are bounded, and have much slower dynamics in comparison with aircraft speed and attitudes, so their derivatives are relatively small. Furthermore, the following assumption is introduced.

Assumption 2. *Induced wake velocities W_x , W_y , and W_z are all bounded, and furthermore, they are piecewise constant, namely $\dot{W}_x = 0$, $\dot{W}_y = 0$, and $\dot{W}_z = 0$.*

The following nonlinear disturbance observer is employed.

$$\widehat{\mathbf{W}} = \boldsymbol{\lambda}_W + \mathcal{T}_W^{-1} \mathbf{X}_P, \quad \dot{\boldsymbol{\lambda}}_W = -\mathcal{T}_W^{-1} \boldsymbol{\lambda}_W - \mathcal{T}_W^{-1} (\mathcal{T}_W^{-1} \mathbf{X}_P + \mathbf{U}_P) \quad (9)$$

where $\mathcal{T}_W = \text{diag}\{\mathcal{T}_{W_x}, \mathcal{T}_{W_y}, \mathcal{T}_{W_z}\} > 0$, $\boldsymbol{\lambda}_W = [\lambda_{W_x}, \lambda_{W_y}, \lambda_{W_z}]^T$, $\mathbf{X}_P = [x_f, y_f, z_f]^T$, $\mathbf{U}_P = [V_f \cos \gamma_f \cos \chi_f, V_f \cos \gamma_f \sin \chi_f, -V_f \sin \gamma_f]^T$, $\widehat{\mathbf{W}} = [\widehat{W}_x, \widehat{W}_y, \widehat{W}_z]^T$ where \widehat{W}_x , \widehat{W}_y , and \widehat{W}_z are estimates of W_x , W_y , and W_z , respectively. It is chosen that $\boldsymbol{\lambda}_W(0) = -\mathcal{T}_W^{-1} \mathbf{X}_P(0)$. Let $\widetilde{W}_x = \widehat{W}_x - W_x$, $\widetilde{W}_y = \widehat{W}_y - W_y$, and $\widetilde{W}_z = \widehat{W}_z - W_z$. Under Assumption 2, one has

$$\dot{\widetilde{W}}_x = -\widetilde{W}_x / \mathcal{T}_{W_x}, \quad \dot{\widetilde{W}}_y = -\widetilde{W}_y / \mathcal{T}_{W_y}, \quad \text{and} \quad \dot{\widetilde{W}}_z = -\widetilde{W}_z / \mathcal{T}_{W_z} \quad (10)$$

According to Lemma 1, \widetilde{W}_x , \widetilde{W}_y , and \widetilde{W}_z can be made arbitrarily small by choosing sufficiently small time constants, even if $\dot{W}_x \neq 0$, $\dot{W}_y \neq 0$, and $\dot{W}_z \neq 0$. To simplify the analysis, it is assumed that $\widetilde{W}_x = \widetilde{W}_y = \widetilde{W}_z = 0$. In light of (9), one has

$$\dot{x}_f = \widehat{V}_f \cos \widehat{\gamma}_f \cos \widehat{\chi}_f, \quad \dot{y}_f = \widehat{V}_f \cos \widehat{\gamma}_f \sin \widehat{\chi}_f, \quad \text{and} \quad \dot{z}_f = -\widehat{V}_f \sin \widehat{\gamma}_f \quad (11)$$

where

$$\begin{cases} \widehat{V}_f = \sqrt{\left(V_f \cos \gamma_f \cos \chi_f + \widehat{W}_x\right)^2 + \left(V_f \cos \gamma_f \sin \chi_f + \widehat{W}_y\right)^2 + \left(-V_f \sin \gamma_f + \widehat{W}_z\right)^2} \\ \widehat{\gamma}_f = -\sin^{-1} \left(\frac{\widehat{W}_z - V_f \sin \gamma_f}{\widehat{V}_f} \right) \\ \widehat{\chi}_f = \chi_f + \sin^{-1} \left(\frac{\widehat{W}_y \cos \chi_f - \widehat{W}_x \sin \chi_f}{V_f \cos \gamma_f} \right) \end{cases}$$

Let $x_e = x_f - x_r$, $y_e = y_f - y_r$, and $z_e = z_f - z_r$. Transform x_e , y_e , and z_e into a new frame.

$$e_x = \cos \widehat{\chi}_f x_e + \sin \widehat{\chi}_f y_e, \quad e_y = -\sin \widehat{\chi}_f x_e + \cos \widehat{\chi}_f y_e, \quad e_z = z_e$$

We have

$$\begin{cases} \dot{e}_x = \widehat{V}_f \cos \widehat{\gamma}_f - V_r \cos \gamma_r \cos e_\chi + \dot{\widehat{\chi}}_f e_y \\ \dot{e}_y = V_r \cos \gamma_r \sin e_\chi - \dot{\widehat{\chi}}_f e_x \\ \dot{e}_z = -\widehat{V}_f \sin \widehat{\gamma}_f + V_r \sin \gamma_r \end{cases} \quad (12)$$

where $e_\chi = \widehat{\chi}_f - \chi_r$. The desired velocity and flight path angle are shown in (13).

$$V_d = (-K_x e_x + V_r \cos \gamma_r \cos e_\chi) / \cos \widehat{\gamma}_f - \delta V, \quad \gamma_d = \sin^{-1} \left(\left(K_z e_z + V_r \sin \gamma_r + \widehat{W}_z \right) / V_f \right) \quad (13)$$

where $K_x, K_z > 0$ are control parameters, and $\delta V = \widehat{V}_f - V_f$. The desired signals V_d and γ_d are passed through a command filter to obtain V_c , γ_c , and their rates. Hence,

$$\begin{bmatrix} \dot{\mathcal{J}}_c \\ \ddot{\mathcal{J}}_c \end{bmatrix} = \begin{bmatrix} 0 & 1 \\ -\omega_{\mathcal{J}}^2 & -2\zeta_{\mathcal{J}}\omega_{\mathcal{J}} \end{bmatrix} \begin{bmatrix} \mathcal{J}_c \\ \dot{\mathcal{J}}_c \end{bmatrix} + \begin{bmatrix} 0 \\ \omega_{\mathcal{J}}^2 \end{bmatrix} \mathcal{J}_d, \quad \mathcal{J} \in \{V, \gamma\} \quad (14)$$

Let $e_V = V_f - V_c$ and $e_\gamma = \gamma_f - \gamma_c$. Note that $\bar{L} = \bar{L}_0 + \bar{L}_\alpha \alpha_f$ where \bar{L}_0 is the lift at $\alpha_f = 0$ and \bar{L}_α is the lift derivative with respect to the angle of attack. According to (7), one has

$$\begin{cases} \dot{e}_V = \underbrace{\frac{T \cos \alpha_f \cos \beta_f - \bar{D}}{m_f}}_{u_V} - g \sin \gamma_f - \dot{V}_c + d_V \\ \dot{e}_\gamma = \underbrace{\frac{(\bar{L}_0 + \bar{L}_\alpha \alpha_f + T \sin \alpha_f) \cos \mu_f - m_f g \cos \gamma_f}{m_f V_f}}_{u_\gamma} - \dot{\gamma}_c + d_\gamma \\ \dot{e}_\chi = \underbrace{\frac{(\bar{L}_0 + \bar{L}_\alpha \alpha_f + T \sin \alpha_f) \sin \mu_f}{m_f V_f \cos \gamma_f}}_{u_\chi} - \dot{\widehat{\chi}}_r + d_\chi \end{cases} \quad (15)$$

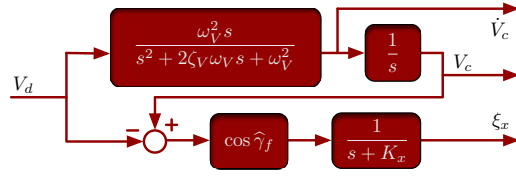


Fig. 3 Command filter and auxiliary system for speed control

where u_V , u_γ , and u_χ are intermediate control inputs, $\hat{\chi}_r$ is the estimation of $\dot{\chi}_r$ by passing χ_r through a 2nd-order filter similar to (5). Two more uncertainty terms $\dot{\hat{\chi}}_r$ and $\dot{\hat{\chi}}_f$ are included in d_χ in (15), where $\dot{\hat{\chi}}_r = \dot{\hat{\chi}}_r - \dot{\chi}_r$ and $\dot{\hat{\chi}}_f = \frac{d}{dt} \sin^{-1} \left(\frac{\hat{W}_y \cos \chi_f - \hat{W}_x \sin \chi_f}{\hat{V}_f \cos \hat{\gamma}_f} \right)$. Hence, d_χ in (15) is re-defined to be $d_\chi = \frac{(L - \bar{L} + \Delta L) \sin \mu_f + (Y + \Delta Y - \cos \alpha_f \sin \beta_f) \cos \mu_f}{m_f V_f \cos \gamma_f} + \dot{\hat{\chi}}_r + \dot{\hat{\chi}}_f + \frac{\hat{W}_{W_y} \cos \mu_f - \hat{W}_{W_z} \sin \mu_f}{m_f V_f \cos \gamma_f}$. Note that χ_r is a smooth signal with bounded derivatives. According to Lemma 2, $\dot{\hat{\chi}}_r$ and its derivative are bounded, so $\dot{\hat{\chi}}_f$ and its derivative are also bounded.

Assumption 3. *The uncertainties and disturbances d_V , d_γ , d_χ , and their derivatives are bounded.*

The following virtual inputs u_V^d , u_γ^d , and u_χ^d are choosing for the error systems (12) and (15).

$$u_V^d = u_{V0}^d - \hat{d}_V + \dot{V}_c, \quad u_\gamma^d = u_{\gamma0}^d - \hat{d}_\gamma + \dot{\gamma}_c, \quad \text{and} \quad u_\chi^d = u_{\chi0}^d - \hat{d}_\chi + \dot{\hat{\chi}}_r \quad (16)$$

where \hat{d}_V , \hat{d}_γ , and \hat{d}_χ are estimates of d_V , d_γ , and d_χ , respectively, and u_{V0}^d , $u_{\gamma0}^d$, and $u_{\chi0}^d$ are

$$u_{V0}^d = -K_V e_V - \frac{c_V \varepsilon_x \cos \hat{\gamma}_f}{H}, \quad u_{\gamma0}^d = -K_\gamma e_\gamma, \quad \text{and} \quad u_{\chi0}^d = -K_\chi e_\chi - \frac{c_\chi e_y V_r \cos \gamma_r \cos \left(\frac{e_\chi}{2} \right)}{H} \quad (17)$$

where K_V , K_γ , K_χ , c_V , $c_\chi > 0$ are control parameters, $H = \sqrt{\varepsilon_x^2 + e_y^2 + 1}$, $\varepsilon_x = e_x - \xi_x$, and $\varepsilon_z = e_z - \xi_z$, where ξ_x and ξ_z in (18) are used to counteract the estimation errors in the filter (14).

$$\dot{\xi}_x = -K_x \xi_x + (V_c - V_d) \cos \hat{\gamma}_f, \quad \dot{\xi}_z = -K_z \xi_z + V_f (\sin \gamma_d - \sin \gamma_f) \quad (18)$$

Shown in Figure 3 is the command filter and auxiliary system for speed control. If one chooses $u_V = u_V^d$, $u_\gamma = u_\gamma^d$, and $u_\chi = u_\chi^d$, there exists

$$\begin{cases} \dot{V}_f = -K_V e_V - c_V \frac{\varepsilon_x \cos \hat{\gamma}_f}{H} + \dot{V}_c - \hat{d}_V + d_V \\ \dot{\gamma}_f = -K_\gamma e_\gamma + \dot{\gamma}_c - \hat{d}_\gamma + d_\gamma \\ \dot{\chi}_f = -K_\chi \sin \left(\frac{e_\chi}{2} \right) - \frac{c_\chi e_y V_r \cos \gamma_r \cos \left(\frac{e_\chi}{2} \right)}{H} + \dot{\hat{\chi}}_r - \hat{d}_\chi + d_\chi \end{cases} \quad (19)$$

Based on (19), the nonlinear disturbance observer is

$$\hat{\mathbf{D}}_D = \boldsymbol{\lambda}_D + \mathcal{T}_D^{-1} \mathbf{X}_D, \quad \dot{\boldsymbol{\lambda}}_D = -\mathcal{T}_D^{-1} \boldsymbol{\lambda}_D - \mathcal{T}_D^{-1} \left(\mathcal{T}_D^{-1} \mathbf{X}_D + \mathbf{U}_D - \hat{\mathbf{D}}_D \right) \quad (20)$$

where $\mathcal{T}_D = \text{diag} \{ \mathcal{T}_V, \mathcal{T}_\gamma, \mathcal{T}_\chi \} > 0$ is a positive definite constant matrix, $\boldsymbol{\lambda}_D = [\lambda_V, \lambda_\gamma, \lambda_\chi]^T$, $\mathbf{X}_D = [V_f, \gamma_f, \chi_f]^T$, $\mathbf{U}_D = [u_{V0}^d, u_{\gamma0}^d, u_{\chi0}^d]^T$, and $\hat{\mathbf{D}}_D = [\hat{d}_V, \hat{d}_\gamma, \hat{d}_\chi]^T$. The uncertainty and

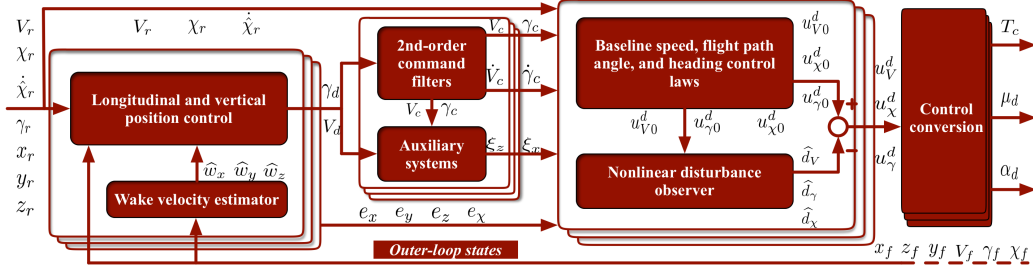


Fig. 4 The outer-loop formation position control structure

disturbance estimates \hat{d}_V , \hat{d}_γ , and \hat{d}_χ need to be fed back to the estimator for the next estimation updates. Combining (17) and (20), one is able to get u_V^d , u_γ^d , and u_χ^d . Hence,

$$\begin{cases} T_c = \frac{m_f(u_V^d + g \sin \gamma_f) + \bar{D}}{\cos \alpha_f \cos \beta_f} \\ \alpha_d = \frac{m_f V_f \sqrt{(u_\gamma^d + \frac{g}{V_f} \cos \gamma_f)^2 + (u_\chi^d)^2} \cos^2 \gamma_f - T \sin \alpha_f - \bar{L}_0}{\bar{L}_\alpha} \\ \mu_d = \tan^{-1} \left(\frac{m_f V_f u_\chi^d \cos \gamma_f}{m_f V_f u_\gamma + m_f g \cos \gamma_f} \right) \end{cases} \quad (21)$$

The entire outer-loop control structure is illustrated in Figure 4. The following assumption is introduced for d_V , d_γ , and d_χ for the stability analysis.

Assumption 4. d_V , d_γ , and d_χ have slow dynamics, and furthermore, $\dot{d}_V \simeq 0$, $\dot{d}_\gamma \simeq 0$, and $\dot{d}_\chi \simeq 0$.

The following error dynamics will be obtained.

$$\begin{cases} \dot{e}_x = \hat{V}_f \cos \hat{\gamma}_f - V_r \cos \gamma_r \cos e_\chi - \dot{\xi}_x + \hat{\chi}_f e_y \\ \dot{e}_y = V_r \cos \gamma_r \sin e_\chi - \dot{\chi}_f e_x \\ \dot{e}_z = -\hat{V}_f \sin \hat{\gamma}_f + V_r \sin \gamma_r - \dot{\xi}_z \end{cases} \quad (22)$$

Assume α_f and μ_f are able to be rapidly stabilized by its inner-loop attitude controller to their desired values α_d and μ_d , respectively. The following theorem holds.

Theorem 1. *If Assumptions 3 and 4 hold, and K_V , K_γ , K_χ , \mathcal{T}_V , \mathcal{T}_γ , \mathcal{T}_χ , c_V , $c_\chi > 0$, $0 < K_x < 2\zeta_V \omega_V$, and $0 < K_z < 2\zeta_\gamma \omega_\gamma$, the proposed outer-loop formation controller given by (16), (17), and (20) will stabilize the outer-loop formation error system composed of (15) and (22), and*

$$\lim_{t \rightarrow \infty} e_x \rightarrow \xi_x, \quad \lim_{t \rightarrow \infty} e_z \rightarrow \xi_z, \quad \text{and} \quad \lim_{t \rightarrow \infty} e_y \rightarrow 0$$

where ξ_x and ξ_z will be ultimately arbitrarily bounded by control parameters ω_V , K_x , and ω_γ , K_z , respectively. If $\xi_x(0) = \xi_z(0) = 0$, there exist

$$\lim_{t \rightarrow \infty} \xi_x \leq \frac{1}{K_x} \|V_c - V_d\|_\infty \quad \text{and} \quad \lim_{t \rightarrow \infty} \xi_z \leq \frac{1}{K_z} \|V_f\|_\infty \|\sin \gamma_d - \sin \gamma_f\|_\infty \quad (23)$$

where $V_c - V_d$ will exponentially converge to $\mathcal{O}\left(\frac{1}{\omega_V}\right)$ and $\lim_{t \rightarrow \infty} \gamma_f - \gamma_d \rightarrow \mathcal{O}\left(\frac{1}{\omega_\gamma}\right)$. Therefore, by tuning ω_V , K_x , and ω_γ , K_z , the ultimate boundaries of e_x and e_z could be regulated accordingly.

Proof. Let $\tilde{d}_i = \hat{d}_i - d_i$ ($i \in \{V, \gamma, \chi\}$). If Assumption 4 holds, and α_f and μ_f are rapidly stabilized to be α_d and μ_d , respectively, it is easily to obtain

$$\dot{\tilde{d}}_V = -\frac{\tilde{d}_V}{\mathcal{T}_V}, \quad \dot{\tilde{d}}_\gamma = -\frac{\tilde{d}_\gamma}{\mathcal{T}_\gamma}, \quad \text{and} \quad \dot{\tilde{d}}_\chi = -\frac{\tilde{d}_\chi}{\mathcal{T}_\chi} \quad (24)$$

Based on (15), (22), and (24), Theorem 1 is proven in two steps. The first step shows $\lim_{t \rightarrow \infty} \varepsilon_x \rightarrow 0$, $\lim_{t \rightarrow \infty} e_y \rightarrow 0$, and $\lim_{t \rightarrow \infty} \varepsilon_z \rightarrow 0$, and thus $\lim_{t \rightarrow \infty} e_x \rightarrow \xi_x$ and $\lim_{t \rightarrow \infty} e_z \rightarrow \xi_z$. The second step demonstrates that ξ_x and ξ_z are uniformly ultimately bounded, which implies e_x and e_z are ultimately bounded. The ultimate boundaries of e_x and e_z are related to control gains.

To show $\lim_{t \rightarrow \infty} \varepsilon_x \rightarrow 0$, $\lim_{t \rightarrow \infty} e_y \rightarrow 0$, and $\lim_{t \rightarrow \infty} \varepsilon_z \rightarrow 0$, we choose

$$\mathbb{V} = H + \frac{\varepsilon_z^2}{2} + 8c_\chi^{-1} \sin^2\left(\frac{e_\chi}{4}\right) + c_V^{-1} \frac{e_V^2}{2} + \frac{e_\gamma^2}{2} + c_\chi^{-1} \frac{\tilde{d}_\chi^2}{2} + c_V^{-1} \frac{\tilde{d}_V^2}{2} + \frac{\tilde{d}_\gamma^2}{2} - 1$$

where $H = \sqrt{\varepsilon_x^2 + e_y^2 + 1}$. Differentiating \mathbb{V} yields

$$\begin{aligned} \dot{\mathbb{V}}_1 &= \frac{\varepsilon_x \dot{\varepsilon}_x}{H} + \frac{e_y \dot{e}_y}{H} + \varepsilon_z \dot{\varepsilon}_z + 2c_\chi^{-1} \sin\left(\frac{e_\chi}{2}\right) \dot{e}_\chi + c_V^{-1} e_V \dot{e}_V + e_\gamma \dot{e}_\gamma + c_\chi^{-1} \tilde{d}_\chi \dot{\tilde{d}}_\chi + \tilde{d}_\gamma \dot{\tilde{d}}_\gamma + c_V^{-1} \tilde{d}_V \dot{\tilde{d}}_V \\ &= -K_x \frac{\varepsilon_x^2}{H} + c_V^{-1} e_V \left(u_V - \dot{V}_c + d_V + \frac{c_V \varepsilon_x \cos \hat{\gamma}_f}{H} \right) - K_z \varepsilon_z^2 + e_\gamma (u_\gamma - \dot{\gamma}_c + d_\gamma) \\ &\quad + 2c_\chi^{-1} \sin\left(\frac{e_\chi}{2}\right) \left(u_\chi - \dot{\hat{\chi}}_r + d_\chi + \frac{c_\chi e_y V_r \cos \gamma_r \cos \frac{e_\chi}{2}}{H} \right) - c_\chi^{-1} \frac{\tilde{d}_\chi^2}{\mathcal{T}_\chi} - c_V^{-1} \frac{\tilde{d}_V^2}{\mathcal{T}_V} - \frac{\tilde{d}_\gamma^2}{\mathcal{T}_\gamma} \end{aligned} \quad (25)$$

Substituting (16) and (17) for corresponding terms in (25) yields

$$\begin{aligned} \dot{\mathbb{V}}_1 &= -c_\chi^{-1} \left[\sin\left(\frac{e_\chi}{2}\right), \tilde{d}_\chi \right] \begin{bmatrix} 2K_\chi & -1 \\ -1 & \frac{1}{\mathcal{T}_\chi} \end{bmatrix} \begin{bmatrix} \sin\left(\frac{e_\chi}{2}\right) \\ \tilde{d}_\chi \end{bmatrix} - c_V^{-1} \left[e_V, \tilde{d}_V \right] \begin{bmatrix} K_V & -0.5 \\ -0.5 & \frac{1}{\mathcal{T}_V} \end{bmatrix} \begin{bmatrix} e_V \\ \tilde{d}_V \end{bmatrix} \\ &\quad - \left[e_\gamma, \tilde{d}_\gamma \right] \begin{bmatrix} K_\gamma & -0.5 \\ -0.5 & \frac{1}{\mathcal{T}_\gamma} \end{bmatrix} \begin{bmatrix} e_\gamma \\ \tilde{d}_\gamma \end{bmatrix} - K_x \frac{\varepsilon_x^2}{H} - K_z \varepsilon_z^2 \end{aligned}$$

If $K_V, K_\chi, K_\gamma, \mathcal{T}_V, \mathcal{T}_\gamma, \mathcal{T}_\chi > 0$, one has

$$\begin{bmatrix} 2K_\chi & -1 \\ -1 & \frac{1}{\mathcal{T}_\chi} \end{bmatrix} > 0, \quad \begin{bmatrix} K_V & -0.5 \\ -0.5 & \frac{1}{\mathcal{T}_V} \end{bmatrix} > 0, \quad \text{and} \quad \begin{bmatrix} K_\gamma & -0.5 \\ -0.5 & \frac{1}{\mathcal{T}_\gamma} \end{bmatrix} > 0$$

Hence, there exists $\dot{\mathbb{V}}_1 \leq 0$ by choosing $K_x > 0$, $K_z > 0$, $c_V > 0$, and $c_\chi > 0$. Therefore, \mathbb{V} is a non-increasing positive definite function, which implies $\mathbb{V}(\infty) \leq \mathbb{V}(0)$ is a finite constant and $\lim_{t \rightarrow \infty} \int_0^t \dot{\mathbb{V}}_1(\tau) d\tau = \mathbb{V}(\infty) - \mathbb{V}(0)$ exists and is finite. Thus, \mathbb{V} is bounded and has a finite limit as $t \rightarrow \infty$, and $\varepsilon_x, e_y, \varepsilon_z, e_\chi, e_V, e_\gamma, \tilde{d}_V, \tilde{d}_\chi$, and \tilde{d}_γ are all bounded as well. Furthermore, $\ddot{\mathbb{V}}_1$ is also bounded, as it is a function of $\varepsilon_x, e_y, \varepsilon_z, e_\chi, e_V, e_\gamma, \tilde{d}_V, \tilde{d}_\chi$, and \tilde{d}_γ . Hence, $\dot{\mathbb{V}}_1$ is uniformly continuous. According to Barbălat's lemma [33], $\lim_{t \rightarrow \infty} \dot{\mathbb{V}}_1 \rightarrow 0$, so $\lim_{t \rightarrow \infty} \varepsilon_x \rightarrow$

0, $\varepsilon_z \rightarrow 0$, $\lim_{t \rightarrow \infty} e_\chi \rightarrow 0$, $\lim_{t \rightarrow \infty} e_V \rightarrow 0$, $\lim_{t \rightarrow \infty} e_\gamma \rightarrow 0$, $\lim_{t \rightarrow \infty} \tilde{d}_V \rightarrow 0$, $\lim_{t \rightarrow \infty} \tilde{d}_\chi \rightarrow 0$, $\lim_{t \rightarrow \infty} \tilde{d}_\gamma \rightarrow 0$. It is obviously that $\lim_{t \rightarrow \infty} e_x \rightarrow \xi_x$ and $\lim_{t \rightarrow \infty} e_z \rightarrow \xi_z$. One could apply Barbălat's lemma to \dot{e}_χ to show $\lim_{t \rightarrow \infty} e_y \rightarrow 0$. Differentiating \dot{e}_χ by time will yield

$$\begin{aligned} \ddot{e}_\chi = & -K_\psi \frac{\dot{e}_\chi}{2} \cos \frac{e_\chi}{2} - \frac{c_\chi \dot{H} e_y V_r \cos \gamma_r \cos \frac{e_\chi}{2}}{H^2} + \frac{c_\chi}{H} \dot{e}_y V_r \cos \gamma_r \cos \frac{e_\chi}{2} + \frac{c_\chi}{H} e_y \dot{V}_r \cos \gamma_r \cos \frac{e_\chi}{2} \\ & - \frac{c_\chi}{H} \dot{\gamma}_r e_y V_r \sin \gamma_r \cos \frac{e_\chi}{2} - \frac{c_\chi}{H} \frac{\dot{e}_\chi}{2} e_y V_r \cos \gamma_r \sin \frac{e_\chi}{2} - \frac{\tilde{d}_\chi}{T_\chi} \end{aligned}$$

Obviously, $\ddot{\chi}_e$ is bounded according to Lemma 1 and Assumptions 1 and 3. Considering $\int \dot{e}_\chi dt = e_\chi$ and $\lim_{t \rightarrow \infty} e_\chi \rightarrow 0$, we have $\dot{\psi}_e \rightarrow 0$ as $t \rightarrow \infty$ in accordance with Barbălat's lemma. According to (15), (16), and (17), $e_y = -\frac{\dot{e}_\chi + K_x e_\chi + \tilde{d}_\chi}{c_\chi V_r \cos \gamma_r \cos \frac{e_\chi}{2}} H$. Since $\lim_{t \rightarrow \infty} \dot{e}_\chi \rightarrow 0$, $\lim_{t \rightarrow \infty} e_\chi \rightarrow 0$, $\lim_{t \rightarrow \infty} \tilde{d}_\chi \rightarrow 0$, $c_\chi V_r \cos \gamma_r \cos \frac{e_\chi}{2} > 0$, and $H > 0$, it is readily to conclude that $\lim_{t \rightarrow \infty} e_y \rightarrow 0$.

The second step shows that ξ_x and ξ_z are uniformly ultimately bounded. From (13), one has

$$V_d = (-K_x e_x + V_r \cos \gamma_r) / \cos \hat{\gamma}_f - \delta V = (-K_x \varepsilon_x - K_x \xi_x + V_r \cos \gamma_r \cos e_\chi) / \cos \hat{\gamma}_f - \delta V \quad (26)$$

Substituting the equation above for V_d in (14) and (18) will generate

$$\begin{bmatrix} \dot{\xi}_x \\ \dot{V}_c \\ \dot{V}_c \end{bmatrix} = \underbrace{\begin{bmatrix} 0 & \cos \hat{\gamma}_f & 0 \\ 0 & 0 & 1 \\ -\frac{K_x \omega_V^2}{\cos \hat{\gamma}_f} & -\omega_V^2 & -2\zeta_V \omega_V \end{bmatrix}}_{\mathbf{A}_v} \begin{bmatrix} \xi_x \\ V_c \\ \dot{V}_c \end{bmatrix} - \begin{bmatrix} \cos \hat{\gamma}_f \\ 0 \\ \omega_V^2 \end{bmatrix} \left(\frac{V_r \cos \gamma_r \cos e_\chi - K_x \varepsilon_x}{\cos \hat{\gamma}_f} + \delta V \right) \quad (27)$$

The characteristic equation of (27) is $s^3 + 2\zeta_V \omega_V s^2 + \omega_V^2 s + K_x \omega_V^2 = 0$. According to the Routh-Hurwitz stability criterion, \mathbf{A}_v is ensured to be Hurwitz all the time, if $0 < K_x < 2\zeta_V \omega_V$. Therefore, the system (27) is input-to-state stable with respect to $\frac{V_r \cos \gamma_r \cos e_\chi - K_x \varepsilon_x}{\cos \hat{\gamma}_f} + \delta V$. According to the previous analysis, ε_x will asymptotically converge to 0. By Assumptions 1 and 2, both δV and $V_r \cos \gamma_r \cos \xi_e$ are uniformly bounded. Since $\hat{\gamma}_f \in (-\frac{\pi}{2}, \frac{\pi}{2})$, $\frac{V_r \cos \gamma_r \cos e_\chi - K_x \varepsilon_x}{\cos \hat{\gamma}_f} + \delta V$ is uniformly bounded, which implies ξ_x is uniformly bounded.

The final boundary of ξ_x is related to ω_V and K_x . If $\xi_x(0) = 0$, there exists $\xi_x \leq \frac{1}{K_x} (1 - e^{-K_x t}) \|V_c - V_d\|_\infty$, so $\lim_{t \rightarrow \infty} \xi_x \leq \frac{1}{K_x} \|V_c - V_d\|_\infty$. Therefore, by tuning K_x , the ultimate boundary of ξ_x could be changed. In addition, ξ_x is bounded-input-bounded-output with respect to $V_c - V_d$, and Lemma 2 indicates that $V_c - V_d$ will exponentially converge to $\mathcal{O}\left(\frac{1}{\omega_V}\right)$. The ultimate boundary of ξ_x can be, therefore, altered by changing ω_V as well. Since $\lim_{t \rightarrow \infty} e_x \rightarrow \xi_x$, the ultimate boundary of e_x could thus be regulated by changing K_x and ω_V .

According to (18), the dynamics of ξ_z are input-to-state stable with respect to $V_f(\sin \gamma_d - \sin \gamma_f)$. Since $V_f(\sin \gamma_d - \sin \gamma_f)$ is bounded, ξ_z is ultimately bounded. According to our previous analysis, one knows that $\lim_{t \rightarrow \infty} \gamma_f \rightarrow \gamma_c$, while γ_c is from a 2nd-order command filter (14). As $\gamma_c - \gamma_d = \mathcal{O}\left(\frac{1}{\omega_\gamma}\right)$, $\lim_{t \rightarrow \infty} \gamma_f - \gamma_d \rightarrow \mathcal{O}\left(\frac{1}{\omega_\gamma}\right)$, and thus $\sin \gamma_d - \sin \gamma_f$ will eventually be limited by certain small boundaries related to ω_γ . Therefore, ξ_z is uniformly ultimately bounded. Choosing $\xi_z(0) = 0$ implies $\xi_z \leq \frac{1}{K_z}(1 - e^{-K_z t}) \|V_f\|_\infty \|\sin \gamma_d - \sin \gamma_f\|_\infty$, so $\lim_{t \rightarrow \infty} \xi_z \leq \frac{1}{K_z} \|V_f\|_\infty \|\sin \gamma_d - \sin \gamma_f\|_\infty$. As $\lim_{t \rightarrow \infty} e_x \rightarrow \xi_x$, $\lim_{t \rightarrow \infty} e_z \rightarrow \xi_z$, and both ξ_x and ξ_z are uniformly ultimately bounded, e_x and e_z will be ultimately bounded, respectively. \square

B. Inner-loop attitude control

The inner-loop dynamics of a follower aircraft in close formation is

$$\begin{cases} \dot{\mu}_f = p \frac{\cos \alpha_f}{\cos \beta_f} + r \frac{\sin \alpha_f}{\cos \beta_f} + \dot{\gamma}_f \cos \mu_f \tan \beta_f + \dot{\chi}_f (\sin \gamma_f + \sin \mu_f \cos \gamma_f \tan \beta_f) \\ \dot{\alpha}_f = q - p \tan \beta_f \cos \alpha_f - r \sin \alpha_f \tan \beta_f - \dot{\gamma}_f \frac{\cos \mu_f}{\cos \beta_f} - \dot{\chi}_f \frac{\sin \mu_f \cos \gamma_f}{\cos \beta_f} \\ \dot{\beta}_f = p \sin \alpha_f - r \cos \alpha_f - \dot{\gamma}_f \sin \mu_f + \dot{\chi}_f \cos \mu_f \cos \gamma_f \\ \dot{p} = \frac{(I_y - I_z)I_z - I_{xz}^2}{I_x I_z - I_{xz}^2} pq + \frac{(I_x - I_y + I_z)I_{xz}}{I_x I_z - I_{xz}^2} pq + \frac{I_z}{I_x I_z - I_{xz}^2} (\mathcal{L} + \Delta \mathcal{L}) + \frac{I_{xz}}{I_x I_z - I_{xz}^2} (\mathcal{N} + \Delta \mathcal{N}) \\ \dot{q} = \frac{I_z - I_x}{(I_x I_z - I_{xz}^2)I_y} pr - \frac{I_{xz}}{(I_x I_z - I_{xz}^2)I_y} (p^2 - r^2) + \frac{1}{(I_x I_z - I_{xz}^2)I_y} (\mathcal{M} + \Delta \mathcal{M}) \\ \dot{r} = \frac{(I_x - I_y)I_x + I_{xz}^2}{I_x I_z - I_{xz}^2} pq - \frac{(I_x - I_y + I_z)I_{xz}}{I_x I_z - I_{xz}^2} rq + \frac{I_{xz}}{I_x I_z - I_{xz}^2} (\mathcal{L} + \Delta \mathcal{L}) + \frac{I_x}{I_x I_z - I_{xz}^2} (\mathcal{N} + \Delta \mathcal{N}) \end{cases} \quad (28)$$

where μ_f is the bank angle, α_f is the angle of attack, β_f is the sideslip angle, p , q , and r are angular rates in the body frame, \mathcal{L} , \mathcal{M} , and \mathcal{N} are moments, while $\Delta \mathcal{L}$, $\Delta \mathcal{M}$, and $\Delta \mathcal{N}$ are the moment disturbances induced by trailing vortices. The presented attitude controller will rapidly stabilize α_f and μ_f to their desired values α_d and μ_d , respectively. Meanwhile, the sideslip angle β_f will be kept to be 0. Regarding the first objective, a command filter is employed again to estimate the derivatives of α_d and μ_d , respectively.

$$\begin{bmatrix} \dot{\mathcal{J}}_c \\ \ddot{\mathcal{J}}_c \end{bmatrix} = \begin{bmatrix} 0 & 1 \\ -\omega_{\mathcal{J}}^2 & -2\zeta_{\mathcal{J}}\omega_{\mathcal{J}} \end{bmatrix} \begin{bmatrix} \mathcal{J}_c \\ \dot{\mathcal{J}}_c \end{bmatrix} + \begin{bmatrix} 0 \\ \omega_{\mathcal{J}}^2 \end{bmatrix} \mathcal{J}_d, \quad \mathcal{J} \in \{\alpha, \mu\} \quad (29)$$

Define $e_\alpha = \alpha_f - \alpha_d$ and $e_\mu = \mu_f - \mu_d$. Let $\mathbf{e}_\Theta = [e_\mu, e_\alpha, \beta_f]^T$, $\Theta_d = [\mu_d, \alpha_d, 0]^T$, $\Theta_c = [\mu_c, \alpha_c, 0]^T$, $\Psi = [\gamma_f, \chi_f]^T$, and $\Omega = [p, q, r]^T$. According to (28), we have

$$\dot{\mathbf{e}}_\Theta = \mathbf{G}\Omega + \mathbf{H}\dot{\Psi} - \dot{\Theta}_d \quad (30)$$

where $\dot{\hat{\Psi}}$ will be estimated by $\hat{\Psi} = [u_\gamma + \hat{d}_\gamma, u_\chi + \hat{d}_\chi]^T$, and

$$\mathbf{G} = \begin{bmatrix} \cos \alpha_f \sec \beta_f & 0 & \sin \alpha_f \sec \beta_f \\ -\cos \alpha_f \tan \beta_f & 1 & -\sin \alpha_f \tan \beta_f \\ \sin \alpha_f & 0 & -\cos \alpha_f \end{bmatrix}, \quad \mathbf{H} = \begin{bmatrix} \cos \mu_f \tan \beta_f & \sin \gamma_f + \sin \mu_f \cos \gamma_f \tan \beta_f \\ -\cos \mu_f \sec \beta_f & -\sin \mu_f \cos \gamma_f \sec \beta_f \\ -\sin \mu_f & \cos \mu_f \cos \gamma_f \end{bmatrix}$$

When Assumptions 3 and 4 hold, $\lim_{t \rightarrow \infty} (u_\gamma + \hat{d}_\gamma) \rightarrow \dot{\gamma}$, $\lim_{t \rightarrow \infty} (u_\chi + \hat{d}_\chi) \rightarrow \dot{\chi}$ as $\lim_{t \rightarrow \infty} \hat{d}_\gamma \rightarrow d_\gamma$ and $\lim_{t \rightarrow \infty} \hat{d}_\chi \rightarrow d_\chi$.

Since Assumption 4 is barely met, $\mathbf{H}(\dot{\Psi} - \dot{\hat{\Psi}})$ is treated as model uncertainties. Additionally, $\dot{\Theta}_d$ is replaced by $\dot{\Theta}_c$ in terms of (29), as it is unavailable. Eventually, the model uncertainties of (30) are $\mathbf{d}_\Theta = \mathbf{H}(\dot{\Psi} - \dot{\hat{\Psi}}) + (\dot{\Theta}_c - \dot{\Theta}_d)$. Define $\mathbf{u}_\Theta = \mathbf{G}\Omega + \mathbf{H} - \dot{\hat{\Psi}}$, so

$$\dot{\mathbf{e}}_\Theta = \mathbf{u}_\Theta + \mathbf{d}_\Theta - \dot{\Theta}_c \quad (31)$$

The desired intermediate virtual inputs to stabilize (31) are proposed in (32).

$$\mathbf{u}_\Theta^d = -\mathbf{K}_\Theta \mathbf{e}_\Theta + \dot{\Theta}_c - \hat{\mathbf{d}}_\Theta \quad (32)$$

where $\mathbf{K}_\Theta = \text{diag}\{K_\mu, K_\alpha, K_\beta\} > 0$ is a gain matrix and $\hat{\mathbf{d}}_\Theta$ is the estimation of \mathbf{d}_Θ , which is from

$$\hat{\mathbf{d}}_\Theta = \boldsymbol{\lambda}_\Theta + \mathcal{T}_\Theta^{-1} \mathbf{e}_\Theta, \quad \dot{\boldsymbol{\lambda}}_\Theta = -\mathcal{T}_\Theta^{-1} \boldsymbol{\lambda}_\Theta - \mathcal{T}_\Theta^{-1} (\mathcal{T}_\Theta^{-1} \mathbf{e}_\Theta + \mathbf{u}_\Theta - \dot{\Theta}_c) \quad (33)$$

where $\mathcal{T}_\Theta = \text{diag}\{\mathcal{T}_\mu, \mathcal{T}_\alpha, \mathcal{T}_\beta\} > 0$ is a diagonal time constant matrix, and $\boldsymbol{\lambda}_\Theta = [\lambda_\mu, \lambda_\alpha, \lambda_\beta]^T$.

Since $\mathbf{u}_\Theta = \mathbf{G}\Omega + \mathbf{H} - \dot{\hat{\Psi}}$, the desired angular rates are given by

$$\Omega_d = \mathbf{G}^{-1} (\mathbf{u}_\Theta^d - \mathbf{H} - \dot{\hat{\Psi}}) \quad (34)$$

where $\Omega_d = [p_d, q_d, r_d]^T$. The commanded angular rates p_c , q_c , and r_c are obtained by (35).

$$\begin{bmatrix} \dot{\mathcal{I}}_c \\ \dot{\mathcal{J}}_c \end{bmatrix} = \begin{bmatrix} 0 & 1 \\ -\omega_{\mathcal{S}}^2 & -2\zeta_{\mathcal{S}} \omega_{\mathcal{S}} \end{bmatrix} \begin{bmatrix} \mathcal{I}_c \\ \dot{\mathcal{I}}_c \end{bmatrix} + \begin{bmatrix} 0 \\ \omega_{\mathcal{S}}^2 \end{bmatrix} \mathcal{I}_d, \quad \mathcal{S} \in \{p, q, r\} \quad (35)$$

where $\mathcal{I}_c(0) = \mathcal{I}_d(0)$ for $\mathcal{S} \in \{p, q, r\}$. Define $\mathbf{e}_\Omega = \Omega - \Omega_c$. According to (28), one has

$$\dot{\mathbf{e}}_\Omega = -\mathbf{I}^{-1} \Omega \times \mathbf{I} \Omega + \mathbf{I}^{-1} (\boldsymbol{\tau} + \Delta \boldsymbol{\tau}) - \dot{\Omega}_c \quad (36)$$

where $\boldsymbol{\tau} = [\mathcal{L}, \mathcal{M}, \mathcal{N}]^T$, $\Delta \boldsymbol{\tau} = [\Delta \mathcal{L}, \Delta \mathcal{M}, \Delta \mathcal{N}]^T$, and \mathbf{I} is the inertia matrix of the aircraft. The control inputs are control surface deflections, including aileron deflection δ_a , elevator deflection δ_e , and rudder deflection δ_r . Let $\boldsymbol{\delta}_u = [\delta_a, \delta_e, \delta_r]^T$, and $\boldsymbol{\tau} = \boldsymbol{\tau}_0 + \mathbf{M}_\tau \boldsymbol{\delta}_u$, where \mathbf{M}_τ is the control derivative matrix and $\boldsymbol{\tau}_0$ is the torque vector at $\boldsymbol{\delta}_u = 0$. Both $\boldsymbol{\tau}_0$ and \mathbf{M}_τ cannot be accurately obtained, so they are approximated using available aerodynamic data from wind tunnel tests. Let $\bar{\boldsymbol{\tau}}_0$ and $\bar{\mathbf{M}}_\tau$ be the approximate results of $\boldsymbol{\tau}_0$ and \mathbf{M}_τ , respectively, so

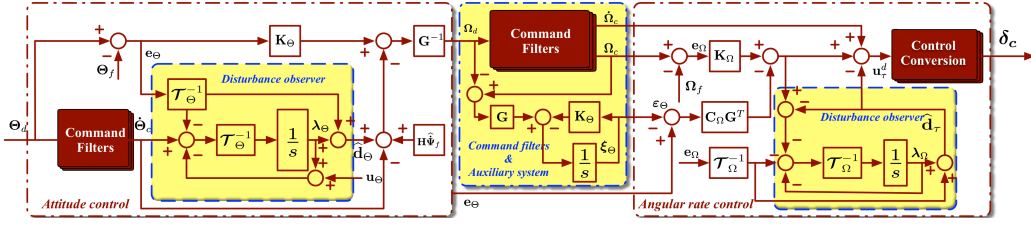


Fig. 5 The inner-loop attitude control structure

$$\bar{\boldsymbol{\tau}} = \bar{\boldsymbol{\tau}}_0 + \bar{\mathbf{M}}_{\boldsymbol{\tau}} \boldsymbol{\delta}_{\mathbf{u}} \quad (37)$$

Let $\mathbf{u}_{\boldsymbol{\tau}} = -\mathbf{I}^{-1} \boldsymbol{\Omega} \times \mathbf{I} \boldsymbol{\Omega} + \mathbf{I}^{-1} (\bar{\boldsymbol{\tau}}_0 + \bar{\mathbf{M}}_{\boldsymbol{\tau}} \boldsymbol{\delta}_{\mathbf{u}}) = [u_p, u_q, u_r]^T$. The error model (36) is rewritten as

$$\dot{\mathbf{e}}_{\boldsymbol{\Omega}} = \mathbf{u}_{\boldsymbol{\tau}} + \mathbf{d}_{\boldsymbol{\tau}} - \dot{\boldsymbol{\Omega}}_c \quad (38)$$

where $\mathbf{d}_{\boldsymbol{\tau}} = \mathbf{I}^{-1} (\boldsymbol{\tau} - \bar{\boldsymbol{\tau}} + \Delta \boldsymbol{\tau})$ is the sum of model uncertainties and formation aerodynamic disturbances. Eventually, the control law for $\mathbf{u}_{\boldsymbol{\tau}}$ is proposed to be

$$\mathbf{u}_{\boldsymbol{\tau}}^d = -\mathbf{K}_{\boldsymbol{\Omega}} \mathbf{e}_{\boldsymbol{\Omega}} - \mathbf{C}_{\boldsymbol{\Omega}} \mathbf{G}^T \boldsymbol{\varepsilon}_{\Theta} - \hat{\mathbf{d}}_{\boldsymbol{\tau}} + \dot{\boldsymbol{\Omega}}_c \quad (39)$$

where $\mathbf{K}_{\boldsymbol{\Omega}} = \text{diag} \{K_p, K_q, K_r\} > 0$ is a diagonal constant gain matrix, $\mathbf{C}_{\boldsymbol{\Omega}} = \text{diag} \{c_p, c_q, c_r\} > 0$ is a constant matrix, $\hat{\mathbf{d}}_{\boldsymbol{\tau}}$ is the estimation of $\mathbf{d}_{\boldsymbol{\tau}}$, and $\boldsymbol{\varepsilon}_{\Theta} = [\varepsilon_{\mu}, \varepsilon_{\alpha}, \varepsilon_{\beta}]^T = \mathbf{e}_{\Theta} - \boldsymbol{\xi}_{\Theta}$ where $\boldsymbol{\xi}_{\Theta}$ is from

$$\dot{\boldsymbol{\xi}}_{\Theta} = -\mathbf{K}_{\Theta} \boldsymbol{\xi}_{\Theta} + \mathbf{G} (\boldsymbol{\Omega}_c - \boldsymbol{\Omega}_d) \quad (40)$$

The uncertainty and disturbance estimator for $\mathbf{d}_{\boldsymbol{\tau}}$ is given by

$$\hat{\mathbf{d}}_{\boldsymbol{\tau}} = \boldsymbol{\lambda}_{\boldsymbol{\Omega}} + \mathcal{T}_{\boldsymbol{\Omega}}^{-1} \mathbf{e}_{\boldsymbol{\Omega}}, \quad \dot{\boldsymbol{\lambda}}_{\boldsymbol{\Omega}} = -\mathcal{T}_{\boldsymbol{\Omega}}^{-1} \boldsymbol{\lambda}_{\boldsymbol{\Omega}} - \mathcal{T}_{\boldsymbol{\Omega}}^{-1} (\mathcal{T}_{\boldsymbol{\Omega}}^{-1} \mathbf{e}_{\boldsymbol{\Omega}} - \mathbf{K}_{\boldsymbol{\Omega}} \mathbf{e}_{\boldsymbol{\Omega}} - \mathbf{C}_{\boldsymbol{\Omega}} \mathbf{G}^T \boldsymbol{\varepsilon}_{\Theta} - \hat{\mathbf{d}}_{\boldsymbol{\tau}}) \quad (41)$$

where $\mathcal{T}_{\boldsymbol{\Omega}} = \text{diag} \{\mathcal{T}_p, \mathcal{T}_q, \mathcal{T}_r\} > 0$ is the time constant matrix. Let $\boldsymbol{\delta}_{\mathbf{c}} = [\delta_{ac}, \delta_{ec}, \delta_{rc}]^T$ be the commanded control surface deflection vector. Eventually, we have

$$\boldsymbol{\delta}_{\mathbf{c}} = \bar{\mathbf{M}}_{\boldsymbol{\tau}}^{-1} (\mathbf{I} \mathbf{u}_{\boldsymbol{\tau}}^d + \boldsymbol{\Omega} \times \mathbf{I} \boldsymbol{\Omega} - \bar{\boldsymbol{\tau}}_0) \quad (42)$$

The inner-loop controller is shown in Figure 5. The following assumption is introduced for the sake of stability analysis.

Assumption 5. Both \mathbf{d}_{Θ} and $\mathbf{d}_{\boldsymbol{\tau}}$ are bounded with slow dynamics, namely $\dot{\mathbf{d}}_{\Theta} \simeq 0$ and $\dot{\mathbf{d}}_{\boldsymbol{\tau}} \simeq 0$.

Define $\tilde{\mathbf{d}}_{\Theta} = \hat{\mathbf{d}}_{\Theta} - \mathbf{d}_{\Theta}$ and $\tilde{\mathbf{d}}_{\boldsymbol{\tau}} = \hat{\mathbf{d}}_{\boldsymbol{\tau}} - \mathbf{d}_{\boldsymbol{\tau}}$. Under Assumption 5, we have

$$\dot{\tilde{\mathbf{d}}}_{\Theta} = -\mathcal{T}_{\Theta}^{-1} \tilde{\mathbf{d}}_{\Theta}, \quad \dot{\tilde{\mathbf{d}}}_{\boldsymbol{\tau}} = -\mathcal{T}_{\boldsymbol{\Omega}}^{-1} \tilde{\mathbf{d}}_{\boldsymbol{\tau}} \quad (43)$$

Lemma 3. If Assumption 5 holds, and $K_{\mu}, K_{\alpha}, K_{\beta}, K_p, K_q, K_r, \mathcal{T}_{\mu}, \mathcal{T}_{\alpha}, \mathcal{T}_{\beta}, \mathcal{T}_p, \mathcal{T}_q, \mathcal{T}_r, c_p, c_q,$ and $c_r > 0$, $\boldsymbol{\varepsilon}_{\Theta}$ and $\mathbf{e}_{\boldsymbol{\Omega}}$ will exponentially converge to zero, namely $\lim_{t \rightarrow \infty} \mathbf{e}_{\Theta} \rightarrow \boldsymbol{\xi}_{\Theta}$, and $\sigma_c - \sigma_d = \mathcal{O} \left(\frac{1}{\omega_{\sigma}} \right)$ and $\boldsymbol{\xi}_{\sigma} = \mathcal{O} \left(\frac{1}{\omega_{\sigma}} \right)$ with $\sigma \in \{p, q, r\}$, so \mathbf{e}_{Θ} is ultimately bounded.

In real implementations, it is only required that \mathbf{d}_Θ , \mathbf{d}_τ , and their derivatives are bounded. If $\dot{\mathbf{d}}_\Theta \simeq 0$ and $\dot{\mathbf{d}}_\tau \simeq 0$ fail to exist, $\xi_\sigma = \mathcal{O}\left(\frac{1}{\omega_\sigma}\right)$ still holds uniformly. However, instead of achieving $\lim_{t \rightarrow \infty} \varepsilon_\Omega \rightarrow 0$, we can only ensure $\|\varepsilon_\Theta - \bar{\varepsilon}_\Theta\| = \mathcal{O}(\epsilon_1)$ and $\|e_\Omega - \bar{e}_\Omega\| = \mathcal{O}(\epsilon_1)$ where ϵ_1 is a certain positive small value related to the time constants of the disturbance observers (33) and (41), and $\bar{\varepsilon}_\Theta$ and \bar{e}_Ω are the attitude tracking errors from the standard backstepping design. The dynamics of $\bar{\varepsilon}_\Theta$ and \bar{e}_Ω are shown in (44). Obviously, there exist $\lim_{t \rightarrow \infty} \bar{\varepsilon}_\Theta \rightarrow 0$ and $\lim_{t \rightarrow \infty} \bar{e}_\Omega \rightarrow 0$. Since $\varepsilon_\Theta = e_\Theta - \xi_\Theta$, e_Θ will be ultimately bounded. This conclusion is summarized in Proposition 1.

$$\dot{\bar{\varepsilon}}_\Theta = -\mathbf{K}_\Theta \bar{\varepsilon}_\Theta + \mathbf{G} \bar{e}_\Omega, \quad \dot{\bar{e}}_\Omega = -\mathbf{K}_\Omega \bar{e}_\Omega - \mathbf{C}_\Omega \mathbf{G}^T \bar{\varepsilon}_\Theta \quad (44)$$

Proposition 1. *Assume \mathbf{d}_Θ , \mathbf{d}_τ , and their derivatives are bounded. The proposed inner-loop attitude control law composed of (32), (33), (34), (35), (39), and (41) will make $\|\varepsilon_\Theta - \bar{\varepsilon}_\Theta\| = \mathcal{O}(\epsilon_1)$ and $\|e_\Omega - \bar{e}_\Omega\| = \mathcal{O}(\epsilon_1)$ uniformly hold, where $\epsilon_1 = \max\{\mathcal{T}_\mu, \mathcal{T}_\alpha, \mathcal{T}_\beta, \mathcal{T}_p, \mathcal{T}_q, \mathcal{T}_r\}$. Furthermore, e_Θ will be uniformly ultimately bounded, and $\|e_\Theta - \bar{e}_\Theta\| = \mathcal{O}(\epsilon_2)$ where $\epsilon_2 = \max\left\{\epsilon_1, \frac{1}{\omega_p}, \frac{1}{\omega_q}, \frac{1}{\omega_r}\right\}$.*

V. Simulation verification

The proposed robust nonlinear close formation controller is validated based on two F-16 aircraft. A high-fidelity model presented in [34] will be employed to simulate the nonlinear dynamics of a F-16 aircraft. The aerodynamic effects by close formation flight are characterized using the aerodynamic model developed in [6]. Note that the aerodynamic data used to build up the nonlinear aircraft model are assumed to be unavailable for the control design. Instead, a global nonlinear parameter modeling technique in [32] is employed to calculate the necessary aerodynamic coefficients and \bar{D} , \bar{L}_0 , \bar{L}_α , $\bar{\tau}_0$, and $\bar{\mathbf{M}}_\tau$. The aircraft geometry and mass parameters are listed in Table 1, while the necessary aerodynamic parameters are given in Table 2. The numerical simulations are carried out at two scenarios. In the first scenario, the robustness of the disturbance observer-based controller is verified by being compared with the control without disturbance observers (DO). In the second scenario, close formation flight is conducted at different velocities with the same group of control parameters to further confirm the efficacy of the proposed design.

Table 1 Aircraft geometry and mass parameters

Parameter	Symbol	Value	Unit	Parameter	Symbol	Value	Unit
Wing area	S	27.87	m^2	Vertical tail height	h_t	3.05	m
Vertical tail area	S_v	5.09	m^2	Quarter-chord sweep angle	Λ_s	0.57	rad
Horizontal tail area	S_h	10.034	m^2	Dihedral angle	Λ_d	0	rad
Wing span	b	9.14	m	Gross mass	m	9295.44	kg
Tail wing span	b_t	5.49	m	Roll moment of inertia	I_x	12874.8	$kg \cdot m^2$
Mean aerodynamic chord	\bar{c}	3.45	m	Pitch moment of inertia	I_y	75673.6	$kg \cdot m^2$
Root chord	c_r	5.02	m	Yaw moment of inertia	I_z	85552.1	$kg \cdot m^2$
Tip chord	c_t	1.07	m	Product moment of inertia	I_{xz}	1331.4	$kg \cdot m^2$

Table 2 Aircraft aerodynamic coefficients

Coefficient	Symbol	Value	Coefficient	Symbol	Value
Zero-lift drag coefficient	C_{D_0}	0.02	Rolling moment coefficient	$C_{\mathcal{L}_{\delta_r}}$	0.02636
Oswald efficiency number	e_o	0.663	Pitching moment coefficient	$C_{\mathcal{M}_0}$	-0.02029
Section lift curve slope	C_{l_α}	5.3	Pitch stiffness	$C_{\mathcal{M}_\alpha}$	0.0466
Lift coefficient	C_{L_0}	0.05	Pitch damping	$C_{\mathcal{M}_q}$	-5.159
Wing lift curve slope	C_{L_α}	5.3	Pitching moment coefficient	$C_{\mathcal{M}_{\delta_e}}$	-0.60123
Vertical tail efficiency factor	c_η	0.95	Weathercock stability derivative	$C_{\mathcal{N}_\beta}$	0.2993
Dihedral effect	$C_{\mathcal{L}_\beta}$	-0.1059	Cross coupling derivative	$C_{\mathcal{N}_p}$	0.02678
Roll damping coefficient	$C_{\mathcal{L}_p}$	-0.4127	Yaw damping coefficient	$C_{\mathcal{N}_r}$	-0.36988
Vertical tail effect coefficient	$C_{\mathcal{L}_r}$	0.0625	Yawing moment coefficient	$C_{\mathcal{N}_{\delta_a}}$	-0.03349
Rolling moment coefficient	$C_{\mathcal{L}_{\delta_a}}$	-0.1463	Yawing moment coefficient	$C_{\mathcal{N}_{\delta_r}}$	-0.081159

A. Scenario 1: With/without disturbance observers

The initial conditions of the leader aircraft are $x_l(0) = 45 \text{ m}$, $y_l = -15 \text{ m}$, $z_l = -5015 \text{ m}$, $V_l = 200 \text{ m/s}$, $\gamma_l = \chi_l = 0 \text{ deg}$. According to the aerodynamic analysis in [6], the optimal relative position vector is selected to be $[-36, 9, 0]^T \text{ m}$. The parameters of the command filters for generating \mathbf{L}_c and estimating are given in Table 3. The initial conditions for the follower aircraft are $x_f(0) = 45$

Table 3 Command filter parameters for \mathbf{L}_c and $\dot{\chi}_r$

Natural frequency	Value	Damping ratio	Value	Natural frequency	Value	Damping ratio	Value
ω_{l_x}	5	ζ_{l_x}	1	ω_{l_y}	5	ζ_{l_y}	1
ω_{l_z}	5	ζ_{l_z}	1	ω_{χ_r}	5	ζ_{χ_r}	1

Table 4 Outerloop control parameters

Parameter	Symbol	Value	Parameter	Symbol	Value	Parameter	Symbol	Value
Time constant	\mathcal{T}_{W_x}	0.8	Control gain	K_x	0.3	Control gain	C_y	10^{-4}
Time constant	\mathcal{T}_{W_y}	0.5	Control gain	K_z	0.2	Control gain	C_z	5×10^{-7}
Time constant	\mathcal{T}_{W_z}	0.4	Control gain	K_V	1.75	Natural frequency	ω_V	8
Time constant	\mathcal{T}_V	0.25	Control gain	K_γ	0.75	Natural frequency	ω_γ	8
Time constant	\mathcal{T}_γ	0.2	Control gain	K_χ	1.75	Damping ratio	ζ_V	1
Time constant	\mathcal{T}_χ	0.2	Control gain	C_x	10^{-5}	Damping ratio	ζ_γ	1

m , $y_f(0) = -15$ m, $z_f(0) = -5015$ m, $V_f(0) = 200$ m/s, $\gamma_f(0) = \chi_f(0) = \mu_f(0) = \beta_f(0) = 0$ deg, $\alpha_f(0) = 2.774$ deg, $p = q = r = 0$ rad/s. The outerloop and innerloop control parameters are presented in Table 4 and 5, respectively. The formation trajectory in the inertial frame is illustrated in Figures 6. From 0 to 35 seconds, the formation trajectory is at level and straight flight. From 35 to 145 seconds, aircraft in close formation are required to make a turn, and meanwhile reduce their altitudes. After 145 seconds, level and straight trajectory is recovered. Shown in Figure 7 are the postures and relative positions of the leader and follower aircraft at four different time instants under the proposed robust nonlinear control. The follower aircraft is initially far away from its optimal position relative to the leader aircraft. Under the proposed robust nonlinear controller, the follower aircraft is able to quickly catch up the optimal relative position. Shown in Figure 8 are highlights of the top and front views of the relative positions between the leader and follower aircraft at 180 seconds.

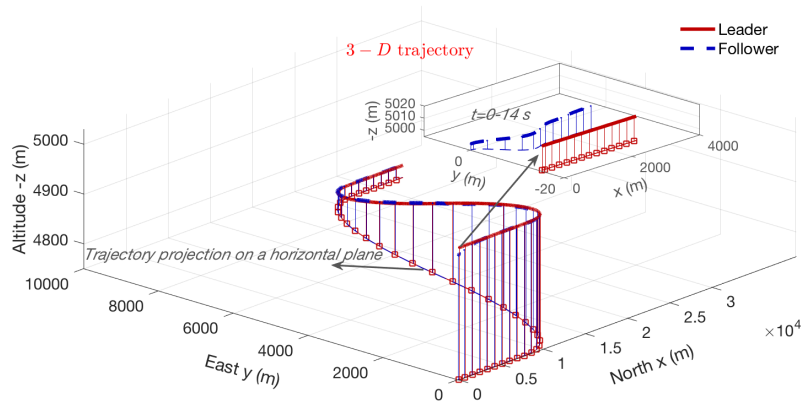


Fig. 6 Formation trajectory

Table 5 Innerloop control parameters

Parameter	Symbol	Value	Parameter	Symbol	Value	Parameter	Symbol	Value
Time constant	\mathcal{T}_μ	0.8	Control gain	K_p	12	Natural frequency	ω_q	5
Time constant	\mathcal{T}_α	0.8	Control gain	K_q	7.5	Natural frequency	ω_r	5
Time constant	\mathcal{T}_β	0.8	Control gain	K_r	7.5	Damping ratio	ζ_μ	1
Time constant	\mathcal{T}_p	0.02	Control gain	c_p	10^{-5}	Damping ratio	ζ_α	1
Time constant	\mathcal{T}_q	0.02	Natural frequency	ω_α	8	Damping ratio	ζ_p	1
Time constant	\mathcal{T}_r	0.02	Natural frequency	ω_μ	8	Damping ratio	ζ_q	1
Control gain	K_μ	5	Control gain	c_r	10^{-5}	Damping ratio	ζ_r	1
Control gain	K_α	5	Control gain	c_q	10^{-5}			
Control gain	K_β	5	Natural frequency	ω_p	25			

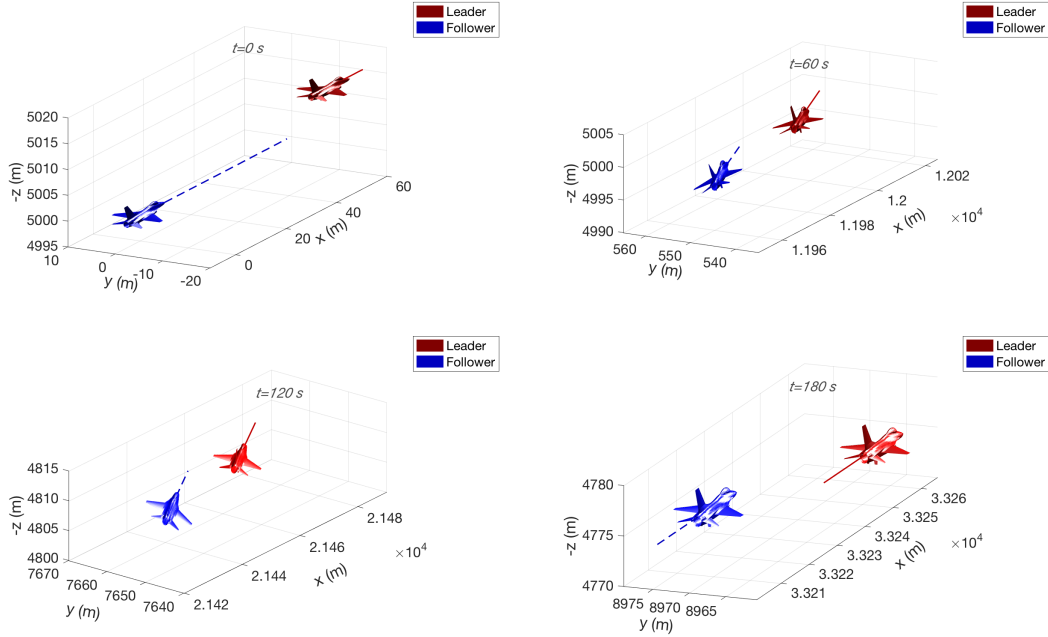


Fig. 7 Aircraft relative positions and postures at different time instants

Two different nonlinear controllers are implemented in the first scenario. One is the proposed robust nonlinear formation controller, the other one is purely the baseline nonlinear formation controller without including disturbance observers (DO). The position tracking errors under the two controllers are shown in Figures 9, 10, and 11. According to [6], close formation flight will fail if the optimal lateral and vertical relative positions cannot be tracked with in 10% wing span, while 90% of the maximum drag reduction could be retained if the position tracking error is kept under

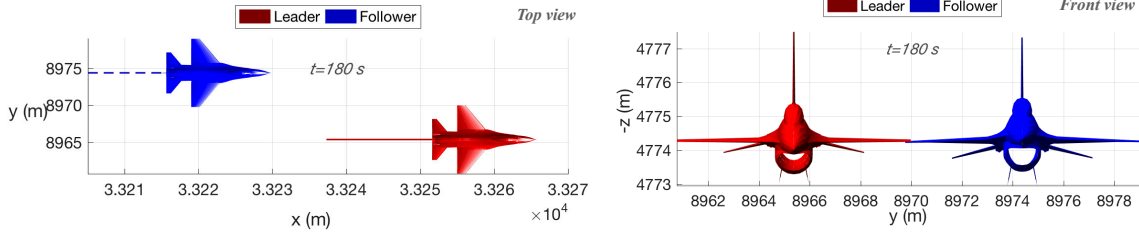


Fig. 8 Top and front view of close formation flight at $t = 180$ s

5% wing span. For efficient close formation flight, it is required that both the lateral and vertical tracking errors are smaller than at least 5% wing span. To show the validness of the proposed design, the regions covered by 5% and 10% wing span are highlighted in Figures 10 and 11. Obviously, the nonlinear control without including disturbance observers failed to achieve reasonable close formation flight, as the vertical position tracking errors are much far away from the region of interest. After incorporating disturbance observers (DO), both the lateral and vertical position tracking errors are confined to be smaller than 5% wing span, so accurate close formation flight is fulfilled. Furthermore, position tracking errors under the proposed robust nonlinear controller would converge to zero when close formation is at level and straight flight. When the leader aircraft is taking maneuvers (35 to 145 s), steady tracking errors are observed for lateral position tracking. The steady tracking errors are under 5% wing span, which implies efficient close formation flight is still guaranteed. Shown in Figures 12, 13, and 14 are tracking errors of speed, flight path angle, and heading angle, respectively. The non-zero lateral steady tracking errors from 35 to 145 s result from the non-zero tracking errors in heading angle control as shown in Figure 14. When leader aircraft is taking maneuvers, the heading angle will have non-zero tracking errors due to the difference between $\dot{\chi}_r$ and $\hat{\dot{\chi}}_r$. In real implementations, the derivative of the reference heading angle χ_r is always unavailable, so a second order filter is introduced to approximate $\dot{\chi}_r$. When the leader aircraft is under level and straight flight, χ_r is constant, which implies $\dot{\chi}_r \equiv 0$. In this case, $\hat{\dot{\chi}}_r$ could be ensured to be equal to $\dot{\chi}_r$, so asymptotical stability is able to be obtained as shown in Figures 9, 10, 11, and 14. However, when the leader aircraft is taking maneuvers, χ_r is not constant, and $\hat{\dot{\chi}}_r$ can only be guaranteed to converge to a certain value close to $\dot{\chi}_r$. The difference between $\hat{\dot{\chi}}_r$ and $\dot{\chi}_r$ might lead to the steady heading tracking errors from 35 to 145 s as shown in Figure 14, which is reflected in lateral position tracking control as given in Figure 10.

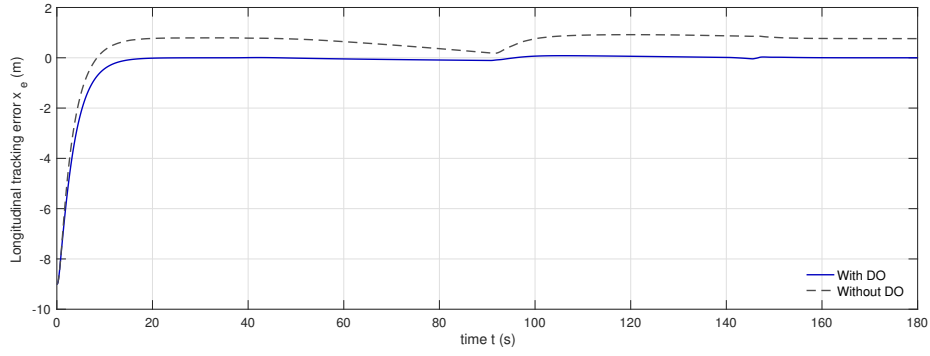


Fig. 9 Longitudinal tracking errors, $x_e = x_f - x_r$ (Scenario 1)

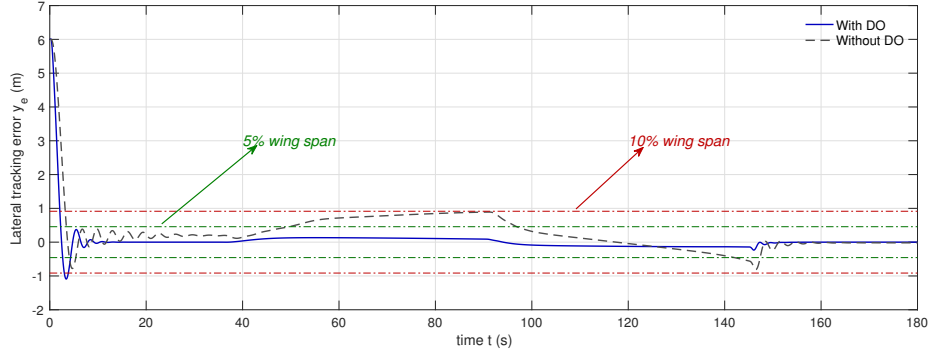


Fig. 10 Lateral tracking errors, $y_e = y_f - y_r$ (Scenario 1)

The inner-loop state responses are summarized in Figure 15. The sideslip angle of the follower aircraft is always kept to be zero by the proposed robust nonlinear formation controller. Shown in Figure 16 are responses of control inputs. As mentioned before, the baseline formation controller without disturbance observers cannot achieve successful close formation flight. The follower aircraft under the baseline controller is eventually one span away from its optimal relative position to the leader aircraft, in which case the influence of the trailing vortices is quite small. Therefore, the steady performance of the follower aircraft by the baseline formation controller is similar to that

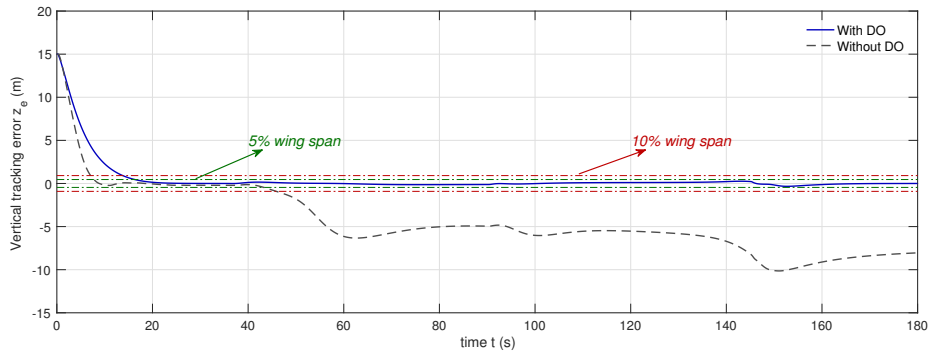


Fig. 11 Vertical tracking errors, $z_e = z_f - z_r$ (Scenario 1)

of an aircraft at solo flight. Compared with the baseline controller, the robust nonlinear controller will eventually have 13.876% decrease in throttle inputs, which implies that around 13.876% energy saving could be obtained by close formation flight.

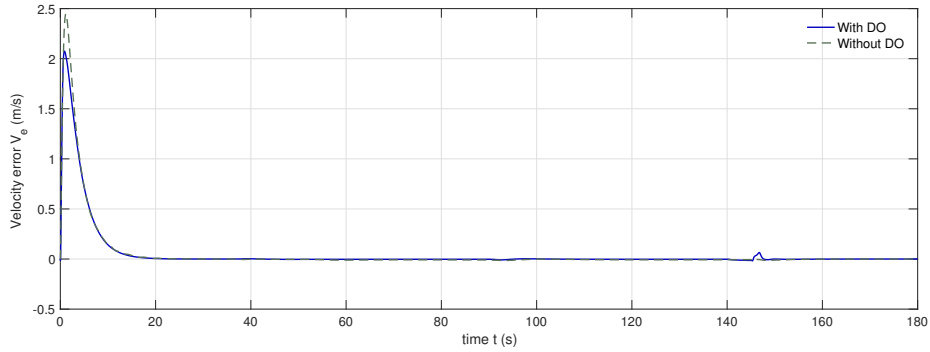


Fig. 12 Speed tracking errors, $V_e = V_f - V_r$ (Scenario 1)

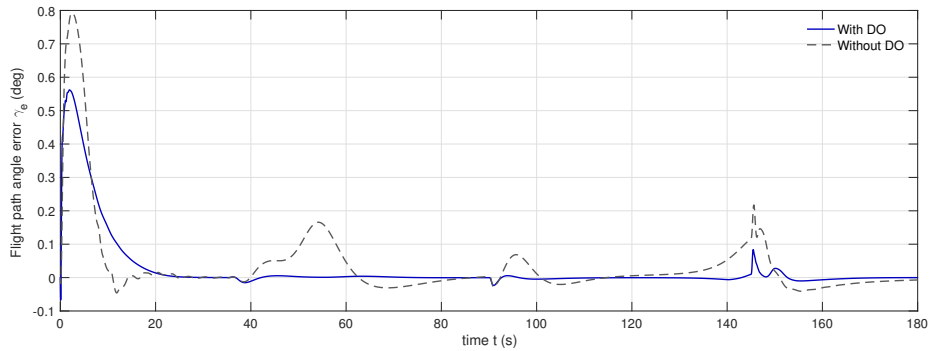


Fig. 13 Flight path angle tracking errors, $\gamma_e = \gamma_f - \gamma_r$ (Scenario 1)

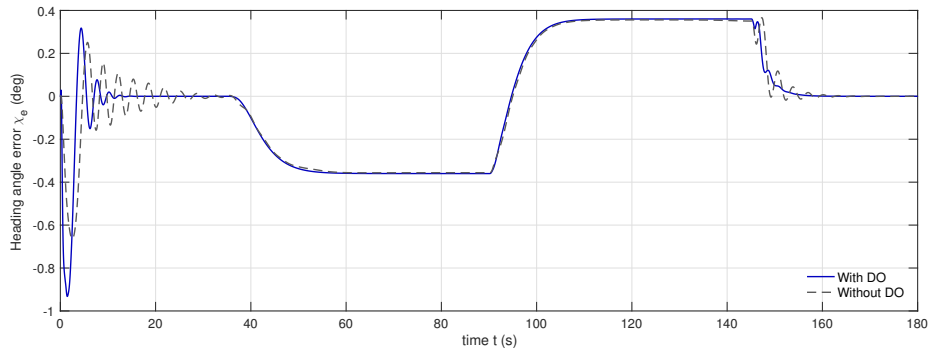


Fig. 14 Heading angle tracking errors, $\chi_e = \chi_f - \chi_r$ (Scenario 1)

B. Scenario 2: Different flight speeds

The efficacy of the proposed robust nonlinear controller is further verified by running the close formation flight under different velocities. All the control parameters, the reference trajectories, and the initial conditions will be same as those at the first scenario. Without loss of generality,

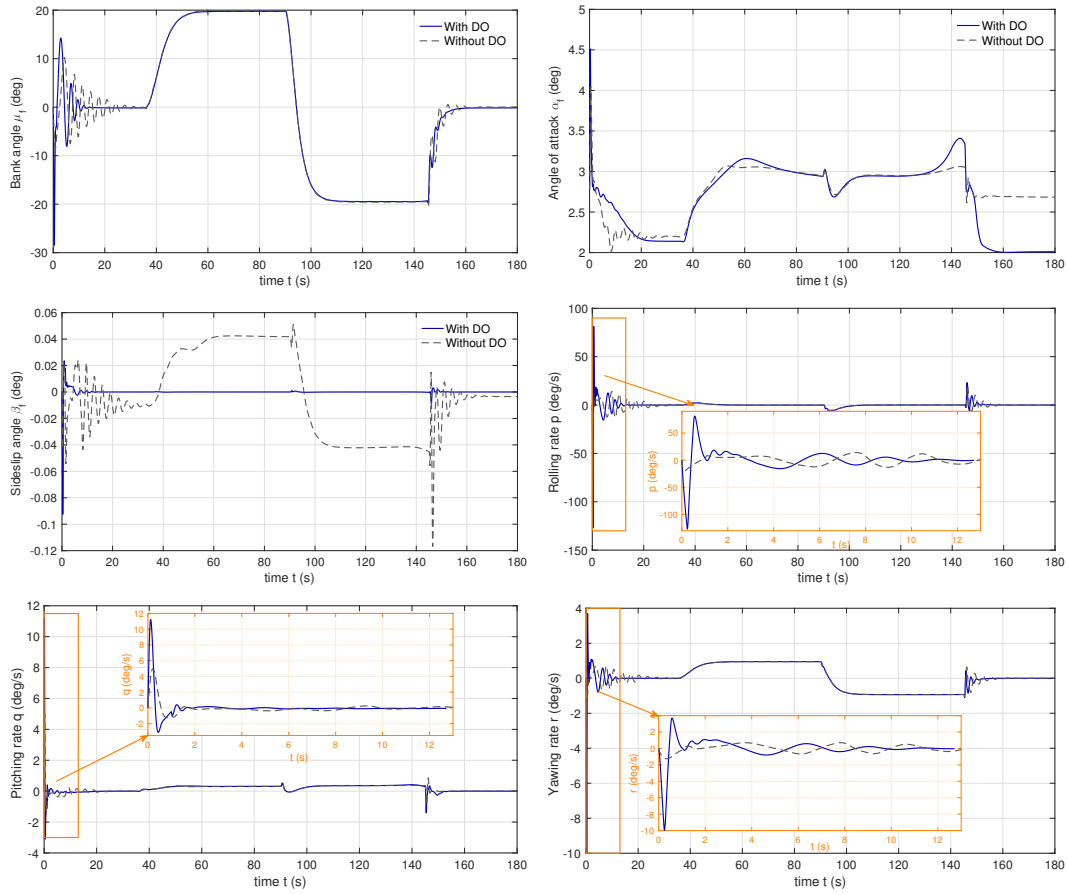


Fig. 15 Inner-loop state responses (Scenario 1)

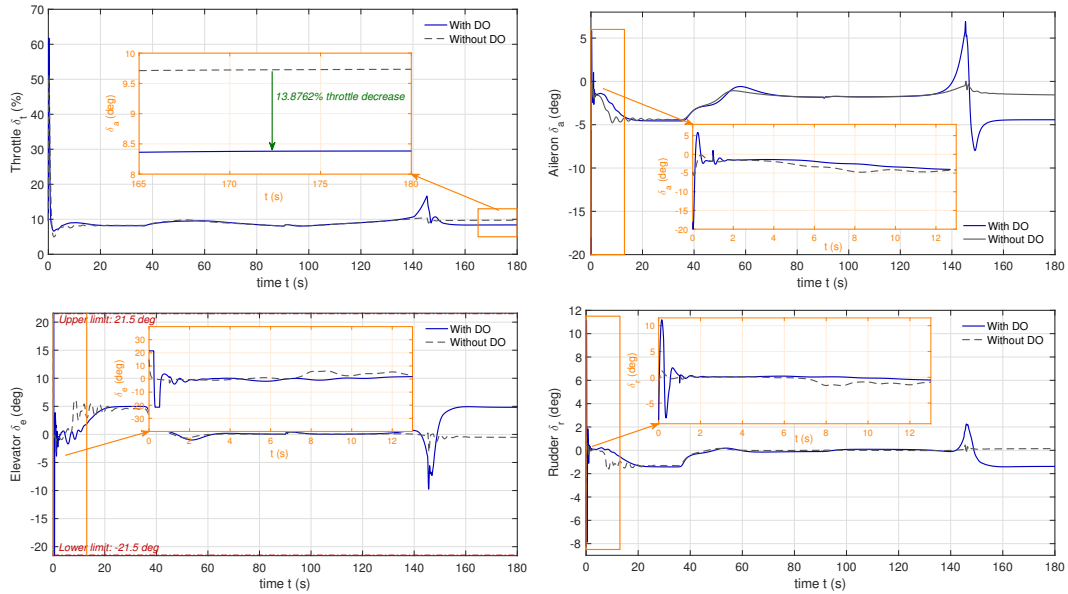


Fig. 16 Actuator responses (Scenario 1)

only position tracking errors and control input responses are given. As compared with a linear controller, nonlinear formation controller can be applied to much wider flight scenarios with stability and performance guaranty. This advantage of the nonlinear controller is demonstrated in Figure

17, 18, and 19. It is observed that the proposed robust nonlinear controller is able to ensure almost the same control performance under different velocities. The control input responses under different velocities are illustrated in Figure 20. Another interesting observation is that increasing speed will result in better performance in lateral position tracking as shown in Figure 18. Explaining this observation is difficult from the nonlinear perspective, but we could analyze it from a linear method at a special case. Assume $V_f = V_r = Const$, $\gamma_f = \gamma_r = 0$, and $\chi_r = 0$. The nonlinear closed outer-loop lateral dynamics are linearized about its equilibrium, which results in

$$\dot{y}_e = V_f e_\chi, \quad \dot{e}_\chi = -\frac{K_\chi}{2} e_\chi - c_y V_f y_e + d_\chi \quad (45)$$

where d_χ denotes any uncertainties, disturbances, or inputs. The transfer function from d_χ to y_e is

$$G(s) = \frac{1}{s^2 + \frac{K_\chi}{2}s + c_y V_f^2} \quad (46)$$

According to the final value theorem, the increase of V_f leads to smaller steady values in y_e as illustrated in Figure 18.

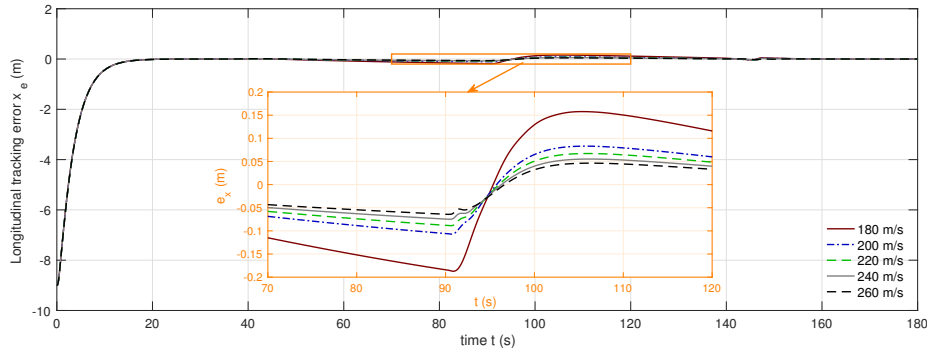


Fig. 17 Longitudinal tracking errors, $x_e = x_f - x_r$ (Scenario 2)

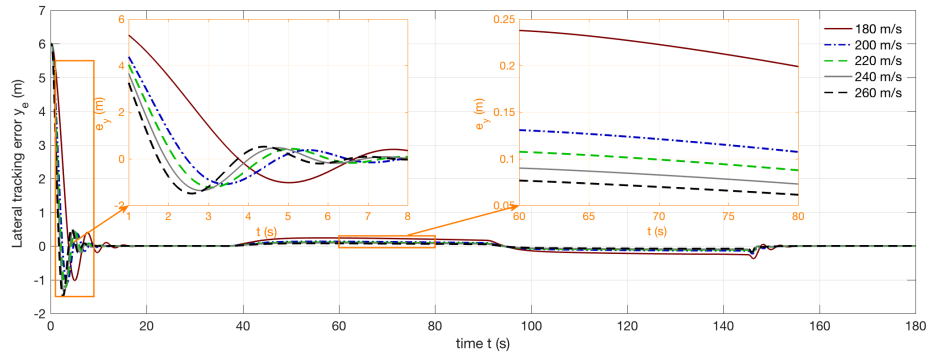


Fig. 18 Lateral tracking errors, $y_e = y_f - y_r$ (Scenario 2)

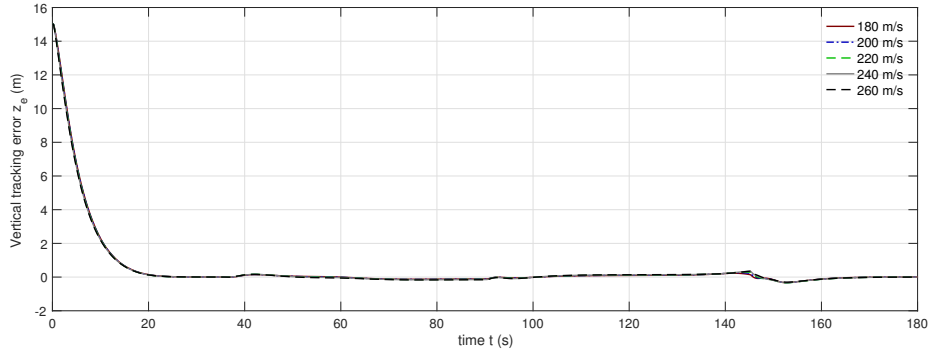


Fig. 19 Vertical tracking errors, $z_e = z_f - z_r$ (Scenario 2)

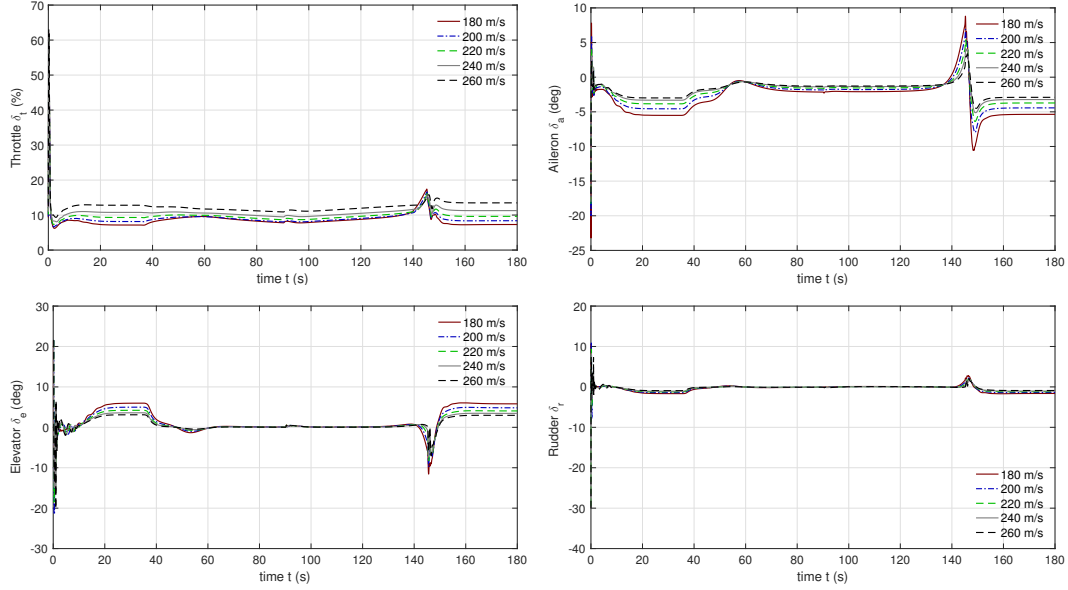


Fig. 20 Actuator responses (Scenario 2)

VI. Conclusions

The paper presented a robust nonlinear controller for autonomous close formation flight under different flight maneuvers. The proposed controller was developed by combining the command filtered backstepping method and the disturbance observation technique. Both inner-loop and outer-loop controllers were designed in this paper. Based on the proposed design, a follower aircraft is able to track its optimal relative position to a leader aircraft under different flight maneuvers. The proposed design was able to be extended to close formation flight of more than three aircraft, though it was described in the scenario of two-aircraft close formation. Enough robustness and high accuracy could be achieved by the presented design. Different numerical simulations were conducted to demonstrate the efficacy of the presented robust nonlinear close formation controller.

Appendix A: Proof of Lemma 1

For (2), the error dynamic equation is

$$\dot{\tilde{d}} = -\frac{1}{\mathcal{T}_d} \tilde{d} + \dot{d} \quad (47)$$

By solving the first-order differential equation (47), one has $\tilde{d}(t) = e^{-\frac{t}{\mathcal{T}_d}} \tilde{d}(0) + \int_0^t e^{-\frac{t-\tau}{\mathcal{T}_d}} \dot{d}(\tau) d\tau$. If choosing $\tilde{d}(0) = 0$, we have $\tilde{d}(0) = -d(0)$. If $\dot{d}(t) \in \mathcal{L}_\infty$,

$$|\tilde{d}(t)| \leq e^{-\frac{t}{\mathcal{T}_d}} |d(0)| + \int_0^t e^{-\frac{t-\tau}{\mathcal{T}_d}} d\tau \|\dot{d}\|_\infty \leq e^{-\frac{t}{\mathcal{T}_d}} |d(0)| + \mathcal{T}_d \left(1 - e^{-\frac{t}{\mathcal{T}_d}}\right) \|\dot{d}\|_\infty \quad (48)$$

Obviously, $|\tilde{d}| \leq \max\{|d(0)|, \mathcal{T}_d \|\dot{d}\|_\infty\}$ globally exists.

For any positive constant ϵ , if $\mathcal{T}_d \|\dot{d}\|_\infty + \epsilon > |d(0)|$, there exists $|\tilde{d}| < \mathcal{T}_d \|\dot{d}\|_\infty + \epsilon \forall t_\epsilon > 0$ according to the global boundedness of $|\tilde{d}|$. If $\mathcal{T}_d \|\dot{d}\|_\infty + \epsilon < |d(0)|$, the first term on the right-hand side of (48) will decrease, while the second term will increase. At certain time t_ϵ , there exists $e^{-\frac{t_\epsilon}{\mathcal{T}_d}} |d(0)| + \mathcal{T}_d \left(1 - e^{-\frac{t_\epsilon}{\mathcal{T}_d}}\right) \|\dot{d}\|_\infty = \mathcal{T}_d \|\dot{d}\|_\infty + \epsilon$. After t_ϵ , the right hand side of (48) will be smaller than $\mathcal{T}_d \|\dot{d}\|_\infty + \epsilon$. By simple mathematical calculation, one has $t_\epsilon = \mathcal{T}_d \ln\left(\frac{|d(0)| - \mathcal{T}_d \|\dot{d}\|_\infty}{\epsilon}\right)$, so the second conclusion of Lemma 1 is obtained. In addition, the estimator error is input-to-state stable with respect to \dot{d} according to (47). Hence, it is obvious that $\lim_{t \rightarrow \infty} \tilde{d} = 0$, if $\lim_{t \rightarrow \infty} \dot{d} = 0$.

Appendix B: Proof of Lemma 2

The following error dynamics are easy to obtain.

$$\dot{\mathbf{e}}_{\mathcal{S}} = \mathbf{A}_{\mathcal{S}} \mathbf{e}_{\mathcal{S}} + \mathbf{B}_{\mathcal{S}} \left(\ddot{\mathcal{J}} + 2\zeta_{\mathcal{S}} \omega_{\mathcal{S}} \dot{\mathcal{J}} \right) \quad (49)$$

where $\mathbf{B}_{\mathcal{S}} = [0, -1]^T$. By choosing $\zeta_{\mathcal{S}}, \omega_{\mathcal{S}} > 0$, $\mathbf{A}_{\mathcal{S}}$ is Hurwitz, which implies $\mathbf{P}_{\mathcal{S}} \mathbf{A}_{\mathcal{S}} + \mathbf{A}_{\mathcal{S}}^T \mathbf{P}_{\mathcal{S}} = -\mathbf{I}$ with $\mathbf{P}_{\mathcal{S}} > 0$. Choose $\mathbb{V} = \mathbf{e}_{\mathcal{S}}^T \mathbf{P}_{\mathcal{S}} \mathbf{e}_{\mathcal{S}}$ as the Lyapunov function for (49), so

$$\lambda_{\min}(\mathbf{P}_{\mathcal{S}}) \|\mathbf{e}_{\mathcal{S}}\|_2^2 \leq \mathbb{V} \leq \lambda_{\max}(\mathbf{P}_{\mathcal{S}}) \|\mathbf{e}_{\mathcal{S}}\|_2^2 \quad (50)$$

If both $\ddot{\mathcal{J}}$ and $\dot{\mathcal{J}}$ are bounded, differentiating \mathbb{V} with respect to time will yield

$$\begin{aligned} \dot{\mathbb{V}} &= \mathbf{e}_{\mathcal{S}}^T (\mathbf{P}_{\mathcal{S}} \mathbf{A}_{\mathcal{S}} + \mathbf{A}_{\mathcal{S}}^T \mathbf{P}_{\mathcal{S}}) \mathbf{e}_{\mathcal{S}} + 2\mathbf{e}_{\mathcal{S}}^T \mathbf{P}_{\mathcal{S}} \mathbf{B}_{\mathcal{S}} \left(\ddot{\mathcal{J}} + 2\zeta_{\mathcal{S}} \omega_{\mathcal{S}} \dot{\mathcal{J}} \right) \\ &\leq -\frac{\mathbb{V}}{\lambda_{\max}(\mathbf{P}_{\mathcal{S}})} + \frac{2\lambda_{\max}(\mathbf{P}_{\mathcal{S}})}{\sqrt{\lambda_{\min}(\mathbf{P}_{\mathcal{S}})}} \|\ddot{\mathcal{J}} + 2\zeta_{\mathcal{S}} \omega_{\mathcal{S}} \dot{\mathcal{J}}\|_\infty \sqrt{\mathbb{V}} \end{aligned}$$

Let $\mathbb{W}(t) = \sqrt{\mathbb{V}}$, so $\dot{\mathbb{W}} = \frac{\dot{\mathbb{V}}}{2\sqrt{\mathbb{V}}}$, when $\mathbb{V} \neq 0$. Hence, $\dot{\mathbb{W}} \leq -\mathbb{W}/(2\lambda_{\max}(\mathbf{P}_{\mathcal{S}})) + \lambda_{\max}(\mathbf{P}_{\mathcal{S}}) \|\ddot{\mathcal{J}} + 2\zeta_{\mathcal{S}} \omega_{\mathcal{S}} \dot{\mathcal{J}}\|_\infty / \sqrt{\lambda_{\min}(\mathbf{P}_{\mathcal{S}})}$. According to the comparison principle (Page 102, [29]), one can get

$$\mathbb{W} \leq e^{-\frac{t}{2\lambda_{\max}(\mathbf{P}_{\mathcal{S}})}} \mathbb{W}(0) + \left(1 - e^{-\frac{t}{2\lambda_{\max}(\mathbf{P}_{\mathcal{S}})}}\right) \frac{2\lambda_{\max}(\mathbf{P}_{\mathcal{S}})}{\sqrt{\lambda_{\min}(\mathbf{P}_{\mathcal{S}})}} \|\ddot{\mathcal{J}} + 2\zeta_{\mathcal{S}} \omega_{\mathcal{S}} \dot{\mathcal{J}}\|_\infty$$

According to (50), $\mathbb{W} \leq \sqrt{\lambda_{\max}(\mathbf{P}_{\mathcal{S}})} \|\mathbf{e}_{\mathcal{S}}\|_2$, so $\mathbb{W}(0) \leq \lambda_{\max}(\mathbf{P}_{\mathcal{S}}) \|\mathbf{e}_{\mathcal{S}}(0)\|_2$. By setting $\mathcal{S}_c(0) = \mathcal{S}(0)$, and $\dot{\mathcal{S}}_c(0) = 0$, one has $\|\mathbf{e}_{\mathcal{S}}(0)\| = |\dot{\mathcal{S}}(0)|$. Eventually,

$$\|\mathbf{e}_{\mathcal{S}}\|_2 \leq \sqrt{\frac{\lambda_{\max}(\mathbf{P}_{\mathcal{S}})}{\lambda_{\min}(\mathbf{P}_{\mathcal{S}})}} e^{-\frac{t}{2\lambda_{\max}(\mathbf{P}_{\mathcal{S}})}} |\dot{\mathcal{S}}(0)| + \left(1 - e^{-\frac{t}{2\lambda_{\max}(\mathbf{P}_{\mathcal{S}})}}\right) \frac{2\lambda_{\max}^2(\mathbf{P}_{\mathcal{S}})}{\lambda_{\min}(\mathbf{P}_{\mathcal{S}})} \|\ddot{\mathcal{S}} + 2\zeta_{\mathcal{S}}\omega_{\mathcal{S}}\dot{\mathcal{S}}\|_{\infty}$$

Therefore, $\mathbf{e}_{\mathcal{S}}$ is uniformly and ultimately bounded. With the consideration of $\|\tilde{\mathcal{S}}\|_2 \leq \|\mathbf{e}_{\mathcal{S}}\|_2$, we are able to conclude that $\tilde{\mathcal{S}}$ is uniformly and ultimately bounded.

The second conclusion of Lemma 2 could be demonstrated by virtue of the perturbation theory. According to (49), the following singularly perturbed system is readily obtained.

$$\frac{1}{\omega_{\mathcal{S}}} \dot{\tilde{\mathcal{S}}}_1 = \tilde{\mathcal{S}}_2, \quad \frac{1}{\omega_{\mathcal{S}}} \dot{\tilde{\mathcal{S}}}_2 = -2\zeta_{\mathcal{S}}\tilde{\mathcal{S}}_2 - \tilde{\mathcal{S}}_1 - \frac{1}{\omega_{\mathcal{S}}} \left(\frac{1}{\omega_{\mathcal{S}}} \ddot{\mathcal{S}} + 2\zeta_{\mathcal{S}}\dot{\mathcal{S}} \right)$$

where $\tilde{\mathcal{S}}_1 = \tilde{\mathcal{S}}$ and $\tilde{\mathcal{S}}_2 = \frac{1}{\omega_{\mathcal{S}}} \dot{\tilde{\mathcal{S}}}$. Obviously, the effect of $\frac{1}{\omega_{\mathcal{S}}} \ddot{\mathcal{S}} + 2\zeta_{\mathcal{S}}\dot{\mathcal{S}}$ will be diminished by increasing the natural frequency $\omega_{\mathcal{S}}$. According to the properties of singularly perturbed system, we readily have $\tilde{\mathcal{S}}_1 = \mathcal{S}_c - \mathcal{S} = \mathcal{O}\left(\frac{1}{\omega_{\mathcal{S}}}\right)$ and $\tilde{\mathcal{S}}_2 = \frac{\dot{\tilde{\mathcal{S}}}}{\omega_{\mathcal{S}}} = \mathcal{O}\left(\frac{1}{\omega_{\mathcal{S}}}\right)$.

Appendix C: Proof of Lemma 3

In light of (31), (36), (32), (38), (39), (40), and (43), one has

$$\begin{cases} \dot{\boldsymbol{\varepsilon}}_{\Theta} = -\mathbf{K}_{\Theta}\boldsymbol{\varepsilon}_{\Theta} + \mathbf{G}\mathbf{e}_{\Omega} - \tilde{\mathbf{d}}_{\Theta} \\ \dot{\mathbf{e}}_{\Omega} = -\mathbf{K}_{\Omega}\mathbf{e}_{\Omega} - \mathbf{C}_{\Omega}\mathbf{G}^T\boldsymbol{\varepsilon}_{\Theta} - \tilde{\mathbf{d}}_{\tau} \end{cases} \quad \begin{cases} \dot{\tilde{\mathbf{d}}}_{\Theta} = -\mathcal{T}_{\Theta}^{-1}\tilde{\mathbf{d}}_{\Theta} \\ \dot{\tilde{\mathbf{d}}}_{\tau} = -\mathcal{T}_{\Omega}^{-1}\tilde{\mathbf{d}}_{\tau} \end{cases} \quad (51)$$

The stability of (51) is shown by picking the Lyapunov function \mathbb{V} as below.

$$\mathbb{V} = \frac{\boldsymbol{\varepsilon}_{\Theta}^T\boldsymbol{\varepsilon}_{\Theta}}{2} + \frac{\mathbf{e}_{\Omega}^T\mathbf{C}_{\Omega}^{-1}\mathbf{e}_{\Omega}}{2} + \frac{\tilde{\mathbf{d}}_{\Theta}^T\tilde{\mathbf{d}}_{\Theta}}{2} + \frac{\tilde{\mathbf{d}}_{\tau}^T\mathbf{C}_{\Omega}^{-1}\tilde{\mathbf{d}}_{\tau}}{2} \quad (52)$$

The derivative of \mathbb{V} is

$$\begin{aligned} \dot{\mathbb{V}} &= \boldsymbol{\varepsilon}_{\Theta}^T \left(-\mathbf{K}_{\Theta}\boldsymbol{\varepsilon}_{\Theta} + \mathbf{G}\mathbf{e}_{\Omega} - \tilde{\mathbf{d}}_{\Theta} \right) - \mathbf{e}_{\Omega}^T\mathbf{C}_{\Omega}^{-1} \left(\mathbf{K}_{\Omega}\mathbf{e}_{\Omega} + \mathbf{C}_{\Omega}\mathbf{G}^T\boldsymbol{\varepsilon}_{\Theta} + \tilde{\mathbf{d}}_{\tau} \right) - \tilde{\mathbf{d}}_{\Theta}^T\mathcal{T}_{\Theta}^{-1}\tilde{\mathbf{d}}_{\Theta} - \tilde{\mathbf{d}}_{\tau}^T\mathbf{C}_{\Omega}^{-1}\mathcal{T}_{\Omega}^{-1}\tilde{\mathbf{d}}_{\tau} \\ &= -\boldsymbol{\varepsilon}_{\Theta}^T\mathbf{K}_{\Theta}\boldsymbol{\varepsilon}_{\Theta} - \boldsymbol{\varepsilon}_{\Theta}^T\tilde{\mathbf{d}}_{\Theta} - \mathbf{e}_{\Omega}^T\mathbf{C}_{\Omega}^{-1}\mathbf{K}_{\Omega}\mathbf{e}_{\Omega} - \mathbf{e}_{\Omega}^T\mathbf{C}_{\Omega}^{-1}\tilde{\mathbf{d}}_{\tau} - \tilde{\mathbf{d}}_{\Theta}^T\mathcal{T}_{\Theta}^{-1}\tilde{\mathbf{d}}_{\Theta} - \tilde{\mathbf{d}}_{\tau}^T\mathbf{C}_{\Omega}^{-1}\mathcal{T}_{\Omega}^{-1}\tilde{\mathbf{d}}_{\tau} \end{aligned}$$

where $\tilde{\mathbf{d}}_{\Theta}$ and $\tilde{\mathbf{d}}_{\tau}$ are both vectors. Let $\tilde{\mathbf{d}}_{\Theta} = [\tilde{d}_{\mu}, \tilde{d}_{\alpha}, \tilde{d}_{\beta}]^T$ and $\tilde{\mathbf{d}}_{\tau} = [\tilde{d}_p, \tilde{d}_q, \tilde{d}_r]^T$, so

$$\begin{aligned} \dot{\mathbb{V}} &= -K_{\mu}\varepsilon_{\mu}^2 - K_{\alpha}\varepsilon_{\alpha}^2 - K_{\beta}\varepsilon_{\beta}^2 - \varepsilon_{\mu}\tilde{d}_{\mu} - \varepsilon_{\alpha}\tilde{d}_{\alpha} - \varepsilon_{\beta}\tilde{d}_{\beta} - \frac{\tilde{d}_{\mu}^2}{T_{\mu}} - \frac{\tilde{d}_{\alpha}^2}{T_{\alpha}} - \frac{\tilde{d}_{\beta}^2}{T_{\beta}} \\ &\quad - \frac{K_p e_p^2}{c_p} - \frac{K_q e_q^2}{c_q} - \frac{K_r e_r^2}{c_r} - \frac{e_p \tilde{d}_p}{c_p} - \frac{e_q \tilde{d}_q}{c_q} - \frac{e_r \tilde{d}_r}{c_r} - \frac{\tilde{d}_p^2}{c_p T_p} - \frac{\tilde{d}_q^2}{c_q T_q} - \frac{\tilde{d}_r^2}{c_r T_r} \end{aligned} \quad (53)$$

It is easy to show that $\dot{\mathbb{V}}_2$ is negative definite, if all control parameters are chosen to be positive.

Hence, $\boldsymbol{\varepsilon}_{\Theta}$ and \mathbf{e}_{Ω} will exponentially converge to zero. To show the second conclusion in Lemma

3, a singular perturbation model is established based on (35) and (40). To simplify the analysis complexity, assume that $\omega_p = \omega_q = \omega_r = \omega_\Omega$ and $\zeta_p = \zeta_q = \zeta_r = \zeta_\Omega$. Define a new variable $\bar{\Omega}_{cdot} = \frac{\dot{\Omega}_c}{\omega_\Omega}$. Therefore, the singular perturbation model is

$$\dot{\xi}_\Theta = -\mathbf{K}_\Theta \xi_\Theta + \mathbf{G}(\Omega_c - \Omega_d) \quad (54a)$$

$$\frac{1}{\omega_\Omega} \dot{\Omega}_c = \bar{\Omega}_{cdot} \quad (54b)$$

$$\frac{1}{\omega_\Omega} \dot{\bar{\Omega}}_{cdot} = -\frac{2\zeta_\Omega}{\omega_\Omega} \bar{\Omega}_{cdot} - (\Omega_c - \Omega_d) \quad (54c)$$

Obviously, the command filter system composed of (54b) and (54c) has much faster dynamics than the auxiliary system (54a), if ω_Ω is chosen to be sufficiently large. The reduced system of (54) is given by $\dot{\bar{\xi}}_\Theta = -\mathbf{K}_\Theta \bar{\xi}_\Theta$ by setting ω_Ω to be infinity, where $\bar{\xi}_\Theta$ is the reduced system state vector. If $\xi_\Theta(0) = \bar{\xi}_\Theta(0) = 0$, $\|\xi_\Theta\| = \mathcal{O}\left(\frac{1}{\omega_\Omega}\right)$ will hold uniformly according to the Tikhonov's theorem, which implies $\xi_\sigma = \mathcal{O}\left(\frac{1}{\omega_\sigma}\right)$. It is easy to get $\sigma_c - \sigma_d = \mathcal{O}\left(\frac{1}{\omega_\sigma}\right)$ according to Lemma 2.

Appendix D: Proof of Proposition 1

When $\dot{\mathbf{d}}_\Theta \neq 0$ and $\dot{\mathbf{D}}_\tau \neq 0$, the closed-loop error dynamics (51) will be rewritten as

$$\begin{cases} \dot{\varepsilon}_\Theta = -\mathbf{K}_\Theta \varepsilon_\Theta + \mathbf{G}e_\Omega - \tilde{\mathbf{d}}_\Theta \\ \dot{e}_\Omega = -\mathbf{K}_\Omega e_\Omega - \mathbf{C}_\Omega \mathbf{G}^T \varepsilon_\Theta - \tilde{\mathbf{d}}_\tau \end{cases} \quad \begin{cases} \mathcal{T}_\Theta \dot{\tilde{\mathbf{d}}}_\Theta = -\tilde{\mathbf{d}}_\Theta - \mathcal{T}_\Theta \dot{\mathbf{d}}_\Theta \\ \mathcal{T}_\Omega \dot{\tilde{\mathbf{d}}}_\tau = -\tilde{\mathbf{d}}_\tau - \mathcal{T}_\Omega \dot{\mathbf{D}}_\tau \end{cases} \quad (55)$$

If the time constants \mathcal{T}_Θ and \mathcal{T}_Ω are chosen to be sufficiently small, (55) will be a standard perturbation model whose reduced system is given in (44). The reduced system (44) is apparently exponentially stable. Since both $\dot{\mathbf{d}}_\Theta$ and $\dot{\mathbf{D}}_\tau$ are bounded, their impact will be diminished by reducing \mathcal{T}_Θ and \mathcal{T}_Ω , respectively. Since $\Omega_c(0) = \Omega_c(0)$ and $\xi_\Theta(0) = 0$, one has $\varepsilon_\Theta(0) = \bar{e}_\Theta(0)$ and $e_\Omega(0) = \bar{e}_\Omega(0)$. According to the Tikhonov's theorem for a standard perturbation model, one is able to conclude that $\|\varepsilon_\Theta - \bar{e}_\Theta\| = \mathcal{O}(\epsilon_1)$ and $\|e_\Omega - \bar{e}_\Omega\| = \mathcal{O}(\epsilon_1)$ will uniformly hold. According to the definition of the order of magnitude, it is easy to find that $\epsilon_1 = \max\{\mathcal{T}_\mu, \mathcal{T}_\alpha, \mathcal{T}_\beta, \mathcal{T}_p, \mathcal{T}_q, \mathcal{T}_r\}$.

Furthermore, with the consideration of (54) and (55), we have

$$\begin{cases} \dot{e}_\Theta = -\mathbf{K}_\Theta e_\Theta + \mathbf{G}e_\Omega + \mathbf{G}(\Omega_c - \Omega_d) - \tilde{\mathbf{d}}_\Theta \\ \dot{e}_\Omega = -\mathbf{K}_\Omega e_\Omega - \mathbf{C}_\Omega \mathbf{G}^T (e_\Theta - \xi_\Theta) - \tilde{\mathbf{d}}_\tau \\ \dot{\xi}_\Theta = -\mathbf{K}_\Theta \xi_\Theta + \mathbf{G}(\Omega_c - \Omega_d) \end{cases} \quad (56)$$

$$\begin{cases} \frac{1}{\omega_\Omega} \dot{\Omega}_c = \bar{\Omega}_{c\dot{d}ot} \\ \frac{1}{\omega_\Omega} \dot{\Omega}_{c\dot{d}ot} = -\frac{2\zeta_\Omega}{\omega_\Omega} \dot{\Omega}_{c\dot{d}ot} - (\Omega_c - \Omega_d) \end{cases} \quad \begin{cases} \mathcal{T}_\Theta \dot{\mathbf{d}}_\Theta = -\tilde{\mathbf{d}}_\Theta - \mathcal{T}_\Theta \dot{\mathbf{d}}_\Theta \\ \mathcal{T}_\Omega \dot{\mathbf{d}}_\tau = -\tilde{\mathbf{d}}_\tau - \mathcal{T}_\Omega \dot{\mathbf{d}}_\tau \end{cases} \quad ll \quad (57)$$

Notice that Eq. (57) will perform as fast dynamics, if ω_Ω is chosen sufficiently large and \mathcal{T}_Θ and \mathcal{T}_Ω are chosen sufficiently small. The reduced system composed of (56) and (57) is still (44). By picking $\xi_\Theta(0) = 0$, one has $e_\Theta(0) = \bar{e}_\Theta$, so $\|e_\Theta - \bar{e}_\Theta\| = \mathcal{O}(\epsilon_2)$ will uniformly hold, where $\epsilon_2 = \max\left\{\epsilon_1, \frac{1}{\omega_p}, \frac{1}{\omega_q}, \frac{1}{\omega_r}\right\}$. In addition, $\lim_{t \rightarrow \infty} \bar{e}_\Theta \rightarrow 0$, so e_Θ will be ultimately bounded.

Acknowledgments

This research work presented in this paper is supported by Natural Science and Engineering Research Council of Canada (NSERC) Discovery Grant 227674.

References

- [1] Lissaman, P. B. S. and Shollenberger, C. A., "Formation Flight of Birds," *Science*, Vol. 68, No. 3934, 1970, pp. 1003–1005.
doi:10.1126/science.168.3934.1003.
- [2] Weimerskirch, H., Martin, J., Clerquin, Y., Alexandre, P., and Jiraskova, S., "Energy Saving in Flight Formation," *Nature*, Vol. 413, 2001, pp. 697–698.
doi:10.1038/35099670.
- [3] Portugal, S. J., Hubel, T. Y., Fritz, J., and et al, "Upwash Exploitation and Downwash Avoidance by Flap Phasing in Ibis Formation Flight," *Nature*, Vol. 413, 2014, pp. 399–402.
doi:10.2514/6.2007-4182.
- [4] Halaas, D. J., Bieniawski, S. R., Whitehead, B. T., Flanzer, T., and Blake, W. B., "Formation Flight For Aerodynamic Benefit Simulation Development and Validation," *Proceedings of the 52nd AIAA Aerospace Sciences Meeting*, National Harbor, MD, USA, Jan. 2014.
doi:10.2514/6.2014-1459, AIAA 2014-0927.
- [5] Kent, T. E. and Richards, A. G., "Analytic Approach to Optimal Routing for Commercial Formation Flight," *Journal of Guidance, Control, and Dynamics*, Vol. 38, No. 10, 2015, pp. 1872–1884.
doi:10.2514/1.G000806.

- [6] Zhang, Q. and Liu, H. H. T., “Aerodynamics Modeling and Analysis of Close Formation Flight,” *Journal of Aircraft*, Vol. 54, No. 6, 2017, pp. 2192–2204.
doi:10.2514/1.C034271.
- [7] Bangash, Z. A., Sanchez, R. P., and Ahmed, A., “Aerodynamics of Formation Flight,” *Journal of Aircraft*, Vol. 43, No. 4, 2006, pp. 907–912.
doi:10.2514/1.13872.
- [8] Cho, H., Lee, S., and Han, C., “Experimental Study on The Aerodynamic Characteristics of a Fighter-Type Aircraft Model in Close Formation Flight,” *Journal of Mechanical Science and Technology*, Vol. 28, No. 8, 2014, pp. 3059–3065.
doi:10.1007/s12206-014-0713-2.
- [9] Ray, R., Cobleigh, B., Vachon, M. J., and John, C. S., “Flight Test Techniques Used to Evaluate Performance Benefits During Formation Flight,” *Proceedings of AIAA Atmospheric Flight Mechanics Conference and Exhibit*, AIAA, Monterey, California, 2002.
doi:10.2514/6.2002-4492, AIAA 2002-4492.
- [10] Pahle, J., Berger, D., Venti, M., Duggan, C., Faber, J., and Cardinal6, K., “An Initial Flight Investigation of Formation Flight for Drag Reduction on the C-17 Aircraft,” *Proceedings of 2012 Atmospheric Flight Mechanics Conference, AIAA AVIATION Forum*, AIAA, Minneapolis, Minnesota, USA, Jan. 2012.
doi:10.2514/6.2012-4802, AIAA 2012-4802.
- [11] Bieniawski, S. R., Clark, R. W., Rosenzweig, S. E., and Blake, W. B., “Summary of Flight Testing and Results for the Formation Flight for Aerodynamic Benefit Program,” *Proceedings of 52nd AIAA Aerospace Sciences Meeting*, AIAA, National Harbor, MD, Jan. 2014.
doi:10.2514/6.2014-1457, AIAA 2014-1457.
- [12] Hanson, C., Pahle, J., Reynolds, J., Andrade, S., and Brown, N., “Experimental Measurements of Fuel Savings During Aircraft Wake Surfing,” *Proceedings of 2018 Atmospheric Flight Mechanics Conference, AIAA AVIATION Forum*, AIAA, Atlanta, Georgia, USA, Jan. 2018.
doi:10.2514/6.2018-3560, AIAA 2018-3560.
- [13] Schumacher, C. J. and Kumar, R., “Adaptive Control of UAVs in Close-Coupled Formation Flight,” *Proceedings of the 2000 American Control Conference*, IEEE, Chicago, Illinois, 2000.
doi:10.1109/ACC.2000.876619.
- [14] Pachter, M., Azzo, J. J. D., and Proud, A. W., “Tight Formation Flight Control,” *Journal of Guidance, Control, and Dynamics*, Vol. 24, No. 2, 2001, pp. 246–254.

doi:10.2514/2.4735.

- [15] Dogan, A. and Venkataramanan, S., “Nonlinear Control for Reconfiguration of Unmanned-Aerial-Vehicle Formation,” *Journal of Guidance, Control, and Dynamics*, Vol. 28, No. 4, 2005, pp. 667–678.

doi:10.2514/1.8760.

- [16] de Almeida, F. A., “Tight Formation Flight with Feasible Model Predictive Control,” *Proceedings of AIAA Guidance, Navigation, and Control Conference*, AIAA, Kissimmee, Florida, U.S.A., 2015, AIAA 2015-0602.

- [17] Binetti, P., Ariyur, K. B., Krstić, M., and Bernelli, F., “Formation Flight Optimization Using Extremum Seeking Feedback,” *Journal of Guidance, Control, and Dynamics*, Vol. 26, No. 1, 2003, pp. 132–142.

doi:10.2514/2.5024.

- [18] Lavretsky, E., Hovakimyan, N., Calise, A., and Stepanyan, V., “Adaptive Vortex Seeking Formation Flight Neurocontrol,” *Proceedings of the 2003 AIAA Guidance, Navigation, and Control Conference and Exhibit*, AIAA, Austin, Texas, Aug. 2003.

doi:10.2514/6.2003-5726, AIAA 2003-5726.

- [19] Chichka, D. F., Speyer, J. L., Fanti, C., and Park, C. G., “Peak-Seeking Control for Drag Reduction in Formation Flight,” *Journal of Guidance, Control, and Dynamics*, Vol. 29, No. 5, 2006, pp. 1221–1230.

doi:10.2514/1.15424.

- [20] Zhang, Q. and Liu, H. H.-T., “Robust Design of Close Formation Flight Control via Uncertainty and Disturbance Estimator,” *Proceedings of 2016 AIAA Guidance, Navigation, and Control Conference, AIAA SciTech Forum*, AIAA, San Diego, California, USA, Jan. 2016.

doi:10.2514/6.2016-2102, AIAA 2016-2102.

- [21] Zhang, Q. and Liu, H. H.-T., “Integrator-Augmented Robust Adaptive Control Design for Close Formation Flight,” *Proceedings of 2017 AIAA Guidance, Navigation, and Control Conference, AIAA SciTech Forum*, Grapevine, TX, USA, Jan. 2017.

doi:10.2514/6.2017-1255, AIAA 2017-1255.

- [22] Zhang, Q. and Liu, H. H. T., “Aerodynamic model-based robust adaptive control for close formation flight,” *Aerospace Science and Technology*, Vol. 79, Aug. 2018, pp. 5–16.

doi:10.1016/j.ast.2018.05.029.

- [23] Singh, S., Pachter, M., Chandler, P., Banda, S., Rasmussen, S., and Schumacher, C., “Input-Output Invertibility and Sliding Mode Control for Close Formation Flying,” *Int. J. Robust Nonlinear Control*, Vol. 10, No. 10, 2000, pp. 779–797.

doi:10.1002/1099-1239(200008)10:10<779::AID-RNC513>3.0.CO;2-6.

- [24] Galzi, D. and Shtessel, Y., "Closed-Coupled Formation Flight Control Using Quasi-Continuous High-Order Sliding-Mode," *Proceedings of the 2007 American Control Conference*, IEEE, New York City, USA, 2007.
- [25] Brodecki, M. and Subbarao, K., "Autonomous Formation Flight Control System Using In-Flight Sweet-Spot Estimation," *Journal of Guidance, Control, and Dynamics*, Vol. 38, No. 6, 2015, pp. 1083–1096. doi:10.2514/1.G000220.
- [26] Farrell, J., Sharma, M., and Polycarpou, M., "Backstepping-Based Flight Control with Adaptive Function Approximation," *Journal of Guidance, Control, and Dynamics*, Vol. 28, No. 6, 2005, pp. 1089–1102. doi:10.2514/1.13030.
- [27] Farrell, J. A., Polycarpou, M., Sharma, M., and Dong, W., "Command Filtered Backstepping," *IEEE Transactions on Automatic Control*, Vol. 54, No. 6, Jun. 2009, pp. 1391–1395. doi:10.1109/TAC.2009.2015562.
- [28] Zhang, Q. and Liu, H. H. T., "UDE-Based Robust Command Filtered Backstepping Control for Close Formation Flight," *IEEE Transactions on Industrial Electronics*, Vol. 65, No. 11, Nov. 2018, pp. 8818–8827. doi:10.1109/TIE.2018.2811367, Early access online, March 12, 2018.
- [29] Khalil, H. K., *Nonlinear Systems*, Prentice Hall, 3rd ed., 2001.
- [30] Sonneveldt, L., Chu, Q., and Mulder, J., "Nonlinear Flight Control Design Using Constrained Adaptive Backstepping," *Journal of Guidance, Control, and Dynamics*, Vol. 30, No. 2, 2007, pp. 322–336. doi:10.2514/1.25834.
- [31] Sonneveldt, L., Oort, E. V., Chu, Q., and Mulder, J., "Nonlinear Adaptive Trajectory Control Applied to an F-16 Model," *Journal of Guidance, Control, and Dynamics*, Vol. 32, No. 1, 2009, pp. 322–336. doi:10.2514/1.38785.
- [32] Morelli, E. A., "Global Nonlinear Parametric Modelling with Application to F-16 Aerodynamics," *Proceedings of the 1998 American Control Conference*, IEEE, Philadelphia, PA, Jun. 1998. doi:10.1109/ACC.1998.703559.
- [33] Ioannou, P. A. and Sun, J., *Robust Adaptive Control*, Prentice-Hall, Inc., 1995.
- [34] Russel, R. S., "Non-linear F-16 simulation using Simulink and Matlab," Tech. rep., Technical report, University of Minnesota, Jun. 2003.